EurJIC
European Journal of Inorganic Chemistry

Minireview
doi.org/10.1002/ejic.202000507

Single-Molecule Magnets

Optimization of Single-Molecule Magnets by Suppression of Quantum Tunneling of the Magnetization

Jan Christian Oldengott,[a] Jürgen Schnack,[b] and Thorsten Glaser*[a]

Abstract: The ligand system triplesalen was rationally designed following requirements for polynuclear 3d single-molecule magnets (SMMs). The essential central part is the C_3 symmetric, *meta*-phenylene bridging unit phloroglucinol for ferromagnetic interactions via the spin-polarization mechanism. The triplesalen-based $[Mn^{III}_6Cr^{III}]^{3+}$ SMMs strongly suppress the quantum tunneling of the magnetization (QTM) but exhibit blocking temperatures not exceeding 2 K. We have analyzed the reason for this behavior and found that the triplesalen ligands are not in the anticipated aromatic phloroglucinol form but in a non-aromatic heteroradialene form. Here we present our strategies to optimize the triplesalen ligand system to suppress the heteroradialene formation and to enforce ferromagnetic interactions. This allowed us to study in detail the influence of exchange coupling on the QTM and relaxation properties of SMMs and provides valuable insights for further rational improvements of our triplesalen ligand system and of SMMs in general.

1. Introduction

Since the revolutionary work of Alfred Werner,[1–3] the focus of coordination chemistry has been on the synthesis of new complexes and in the exploration of their structures and properties and eventually their functions. The gain of such increasing knowledge allowed the establishment of correlations between structure of the complexes and their function (structure-function correlations). A famous example is the fundamental magneto-structural correlation of Hatfield and Hodgson,[4] or the insightful development of homogeneous salen Mn^{III} catalysts for the enantioselective epoxidation of unfunctionalized olefins.[2,3,5]

The research philosophy of our group is based on the application of such valuable structure-function correlations, established in the first century of coordination chemistry, for the rational design of functional supramolecular complexes (Scheme 1). It is our motivation to evaluate how far we can design functional complexes from scratch that can be rationally optimized in improved second or higher generations of ligands and/or complexes. Our starting point is a function/property that we want to create. The targeted structure is then rationally designed using established structure-function correlations. These targeted structures are mainly polynuclear complexes with specific requirements for the bridging modes and e.g. for the relative spatial orientations of the coordination polyhedra and their principal axes. As the rational design is not based on existing complexes, these requirements can usually not be fulfilled by existing ligand systems but demand the development and syntheses of new ligand systems. Due to the specific requirements these ligand systems are generally large multidentate and highly directional ligands requiring elaborated organic synthe-

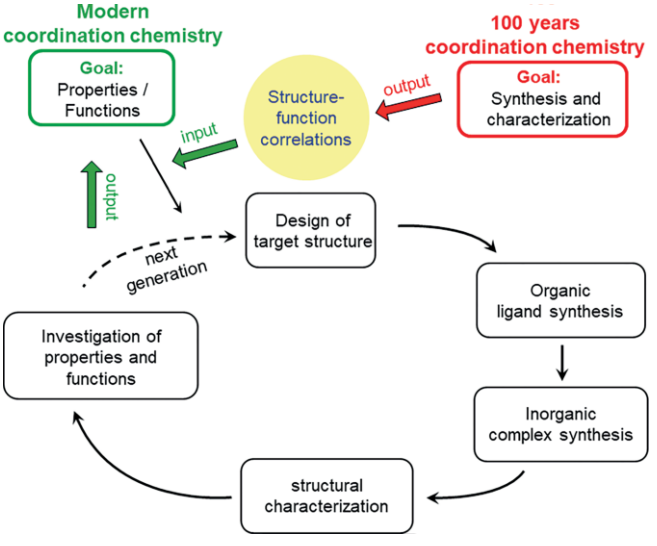

Scheme 1. Research strategy in modern coordination chemistry aiming at properties and functions, while the goal in classic coordination chemistry was the synthesis and characterization of new complexes.

[a] Dr. J. C. Oldengott, Prof. Dr. T. Glaser
Lehrstuhl für Anorganische Chemie I, Fakultät für Chemie,
Universität Bielefeld,
Universitätsstr. 25, 33615 Bielefeld, Germany
E-mail: thorsten.glaser@uni-bielefeld.de
http://www.uni-bielefeld.de/chemie/ac1chair
[b] Prof. Dr. J. Schnack
Fakultät für Physik, Universität Bielefeld,
Universitätsstr. 25, 33615 Bielefeld, Germany
ORCID(s) from the author(s) for this article is/are available on the WWW under https://doi.org/10.1002/ejic.202000507.

This manuscript is part of the Special Collection Pincer Chemistry and Catalysis.

Minireview
doi.org/10.1002/ejic.202000507

ses. Thus, the major part of the synthetic work in our group is the realization of former unknown ligand systems. After the hopefully successful synthesis, the ligands are used for the syntheses of the anticipated complexes, followed by their structural characterization. This allows finally the evaluation of the anticipated property or function. In an ideal situation, this first generation of ligands would provide the complexes with the anticipated property/function. As ideal situations do not exist, the rational improvement of the ligands/complexes of the second generation using the newly generated structure-function correlation is an intellectual challenge. Here, a modular assembly of the ligand system of the first generation facilitates the access to the second-generation ligands, despite the ligand system must be generally reconsidered for the next generation.

In the beginning our group was inspired by a quote of the late Olivier Kahn: "The normal trend for the molecular state is the pairing of electrons [•••] with the cancellation of the electron spin. The design of a molecule-based magnet requires that this trend be successfully opposed."[6] and was mainly focused on the rational design of complexes with ferromagnetic interaction between the paramagnetic metal ions.[7,8,9,10–17] To enforce ferromagnetic ground states, we have been investigating the application of well-known mechanisms:

(*i*) spin-polarization,[18,19]

(*ii*) the orthogonality of magnetic orbitals,[20] and

(*iii*) the double-exchange mechanism.[21]

In the meantime, our group uses this rational design approach also for the development of DNA binding complexes that bind to the phosphates of the DNA backbone instead of usually targeted nucleobases,[22] of C–H activating and water oxidizing catalysts,[23] and single-molecule magnets (SMMs),[24–26] which is the scope of this micro-review.

2. Single-Molecule Magnets

Single-molecule magnets (SMMs) are a class of molecules that show a hysteresis in their magnetization of pure molecular origin. Below a blocking temperature T_B, SMMs keep a remanent magnetization after an applied external magnetic field is switched off.[27–29] All paramagnetic samples show a stabilization of the M_S = -S_t substate by application of a magnetic field via the Zeeman effect resulting in a macroscopic magnetization. While normal paramagnetic samples relax to an unordered distribution with an almost instantaneous loss of magnetization, an energy barrier for magnetization reversal U in SMMs slows this relaxation down, which results in a remnant magnetization at zero field for a specific time. This effect was discovered almost 30 years ago on the manganese complex $[Mn_{12}O_{12}(OAc)_{16}(H_2O)_4]$, **$Mn_{12}$**.[27,30] The Mn^{III} and Mn^{IV} ions couple via superexchange pathways to a high spin ground state of S_t = 10. The local magnetic anisotropy D_i of the Mn^{III} ions contribute to the anisotropy of the spin ground state D_{S_t}. The height of the barrier U is the energy difference between the $M_S = \pm S_t$ and M_S = 0 states, which is $U = D_{S_t} \cdot S_t^2$ (for integer spins; for half-integer spin states, the top of the barrier are the $M_S = \pm 1/2$ states and the height is given by D_{S_t} (S_t^2 – 1/4)). For **Mn_{12}**, a value of $U_{eff} \approx$ 65 K was obtained[27] and an open hysteresis of the magnetization with a large opening at zero magnetic field could be observed up to 4 K.[31]

The discovery of **Mn_{12}** and its SMM properties opened an ever-increasing interest and continuing research in this field. In the beginning, the focus was on polynuclear transition metal complexes. The first improvement since **Mn_{12}** was the family of **Mn_6** complexes with salicylaldoximine ligands,[32] where the variations in SMM properties can be rationally explained.[33] Then, a report of Ishikawa and co-workers on a mononuclear

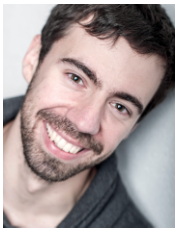

Jan Oldengott studied chemistry at the RWTH Aachen University and obtained his M. Sc. on nitrogen-rich solid-state compounds in 2012. He moved to Bielefeld University, focusing on single-molecule magnets under the guidance of Prof. T. Glaser, and obtained his PhD in 2017. From 2018 to 2019 he joined the group of Prof. A. Llobet (ICIQ, Tarragona, Spain) as a DFG postdoc-fellow. Late 2019 he returned to Bielefeld University as senior scientist in the group of Prof. T. Glaser to work on molecular magnetism, 2D polymers, electrochemistry, water oxidation catalysis, and X-ray crystallography.

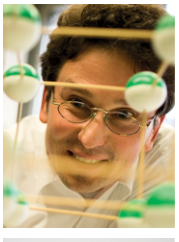

Jürgen Schnack studied physics at the Technical Universities of Dresden and Darmstadt. He obtained his Diploma in 1993 and his PhD in 1996 both in Theoretical Nuclear Physics. His research field changed to molecular magnetism in the late 1990s. He undertook his habilitation at Osnabrück University in 2001 and since 2007 he has been Professor of Theoretical Physics at Bielefeld University. He served as the Dean of the Faculty of Physics in Bielefeld 2017–2019.

Thorsten Glaser studied chemistry in Bochum and obtained his Dr. rer. nat. in 1997 with Prof. K. Wieghardt at the Max-Planck-Institut, Mülheim. After postdoctoral work with Professors E. I. Solomon and K. O. Hodgson at Stanford University, he started his independent research in 2000 at the Wesfälische Wilhelms Universität Münster. Since 2005, he is full professor for inorganic chemistry at Bielefeld University. His research is focused on the rational design of functional transition metal complexes. His current research projects are mainly in bioinorganic chemistry especially biomimetic oxidation catalysis and DNA recognition, in magnetochemistry, especially single-molecule magnets and 2D monolayers, and in water oxidation catalysis.

Tb^{III} complex with two phthalocyanine ligands that exhibits a barrier of 330 K[34] changed the focus to lanthanide complexes,[35,36] later also to actinide complexes[37] and to mononuclear 3d metal ion complexes.[38] This research provided ever increasing anisotropy barriers with values up to 1815 K[36] while the accompanying hysteresis loops could mostly only be observed at lower temperatures than for **Mn_{12}**, and they close at zero magnetic field.[39] Recently, there has been sensational success in increasing the blocking temperature[40] with a record of 80 K for a Dy^{III} metallocene complex.[41]

However, despite this success the explanation, why the properties of particular SMMs are so outstanding while other closely related complexes are not, is not straightforward and is under actual research.[42] The reason for the discrepancy was found in the quantum nature of the molecules:[43,44] besides the thermal pathway over the top of the anisotropy barrier *U*, there are also pathways through the barrier. These can be either coherent transitions (quantum tunneling of the magnetization, QTM) or thermal transitions using lattice vibrations. These short cuts lower the anisotropy barrier *U* to an effective anisotropy barrier U_{eff} that is relatively easily accessible by frequency-dependent AC magnetization measurements. It appears that the QTM is not only difficult to control but also difficult to suppress.

The greatest improvements in SMM research have been obtained in a more serendipity-oriented approach[45] or by variation of known SMMs.[46] Our approach in SMM research has been the question whether we can rationally design a new family of polynuclear 3d SMMs[47] that can be rationally improved with regards to our general approach described above. In this respect, we are far away from the increasing numbers of records obtained with lanthanide complexes, but our driving force is the pure intellectual challenge whether rationally designed SMMs with 3d metal ions are feasible.

3. Rational Design of SMMs with the Triplesalen Ligand System

The height of the anisotropy barrier $U = D_{S_t} \cdot S_t^2$ and the QTM pathways through the barrier,[43,44] provide three requirements that must be the basis for a rational design of polynuclear transition metal SMMs:

(*i*) a high spin ground state S_t,

(*ii*) a strong anisotropy of this ground state, namely the total zero-field splitting , and

(*iii*) the suppression of QTM.

We have already reviewed our rational design for generating a high spin ground state S_t with a strong anisotropy and for the suppression of QTM.[25,26] Thus, only a brief summary is provided here.

(*i*) A report using 1,3,5-trihydroxybenzene (phloroglucinol) as a ferromagnetic coupler between three Mo^{V} ions via the spin-polarization mechanism[48] caught our interest to use extended phloroglucinol ligands with chelating pendant arms in 2,4,6-position as general ferromagnetic coupler, also between 3d metal ions.[7]

(*ii*) The anisotropy of polynuclear complexes D_{S_t} mainly originates from the projection of the single-site anisotropy tensors $\boldsymbol{D}_i$ onto the total spin ground state besides from some anisotropic and antisymmetric exchange.[49,50] The magnetic anisotropy of transition metal ions originates from orbital angular momentum contributions to the magnetic moment mainly from spin-orbit coupling in distorted ligand fields as in the Mn^{III} ions of **Mn_{12}**. In a tetragonal ligand field, $D_{Mn^{III}}$ is directly proportional to the tetragonal distortion.[49,51] In this respect, we have chosen the well investigated salen ligand to generate a strongly tetragonal ligand field.[52]

(*iii*) QTM originates in zero-field from coherent transitions between the $M_S = \pm S_t$ substates and in applied fields, when the Zeeman effect brings two other M_S substates close in energy.[29,53] An equation for the tunneling probability between these substates (P_{M_S,M'_S}) has been obtained using the theoretical treatment of Landau, Zener, and Stückelberg.[54] This probability is related to the tunnel splitting Δ, which is caused by the mixing of M_S substates (Equation 1).[53,55]

$$P_{M_S,M'_S} \propto 1 - \exp[\Delta^2] \qquad (1)$$

The mixing of M_S substates is induced by transversal field components, which may arise from the rhombicity E_{S_t}/D_{S_t} of S_t, stray fields of neighboring molecules, hyperfine interactions, or the noncollinearity of local $\boldsymbol{D}_i$ tensors. While a spin of pure axial symmetry has no mixing of its M_S substates, a rhombic term E_{S_t} induces mixing, resulting in a tunnel splitting Δ (Equation 2) and thereby QTM.

$$\Delta \propto \left(\frac{E_{S_t}}{D_{S_t}}\right)^{S_t} \qquad (2)$$

Thus, the combination of minimizing E_{S_t}/D_{S_t} while maximizing S_t should reduce QTM in SMMs. Here it is important to note, that the rhombicity E_{S_t}/D_{S_t} is zero for a symmetry of at least C_3 but that D_{S_t} vanishes completely for cubic symmetry.[56]

Thus, in a rational design, we have combined these requirements in the hybrid ligand triplesalen (Scheme 2).[8] Three salen-like coordination environments to induce magnetic anisotropy are bridged by the C_3 symmetric ferromagnetic coupling unit phloroglucinol. From a synthetic perspective, our first triplesalen ligands H_6talen^X were based on salen subunits with central ketimine and terminal aldimine functions and an unsymmetrical ethylene spacer.[57] The *tert*-butyl derivative $H_6talen^{t\text{-}Bu2}$ turned out to be the best-suited one.

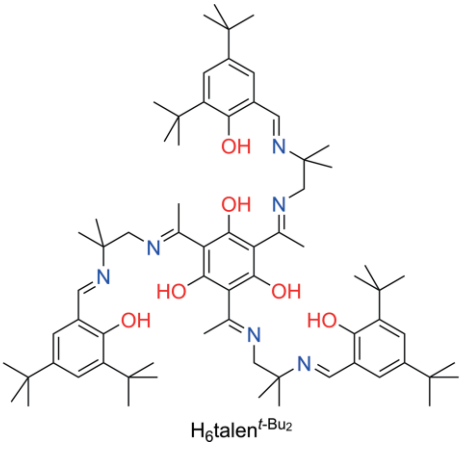

$H_6talen^{t\text{-}Bu2}$

Minireview
doi.org/10.1002/ejic.202000507

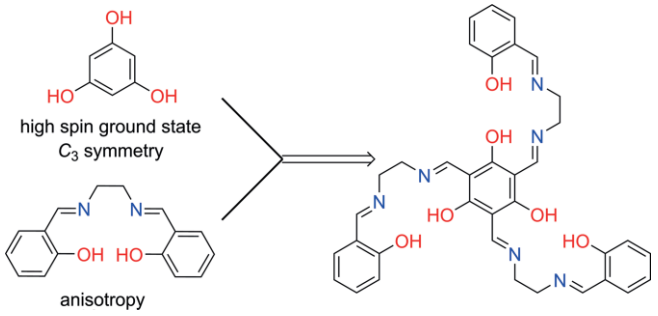

Scheme 2. Rational design of the triplesalen ligand system.

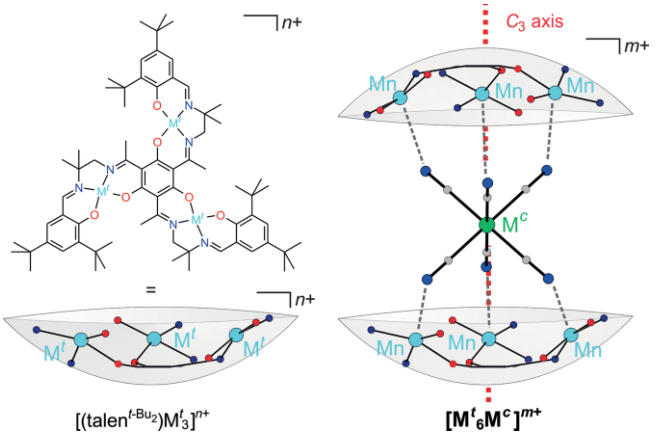

Scheme 3. Building block approach of the heptanuclear complexes $[M^t_6M^c]^{n+}$ from two bowl-shaped trinuclear triplesalen complexes and one hexacyanometallate.

4. Synthesis and Properties of the Heptanuclear $[M^t_6M^c]^{3+}$ Single-Molecule Magnets

The trinuclear complexes of the ligand $H_6talen^{t\text{–}Bu2}$ show a ligand folding resulting in a bowl-shaped molecular structure (Scheme 3 bottom left).[14] Two of these bowl-shaped units have the tendency to dimerise, mainly driven by van-der-Waals interactions between the *tert*-butyl phenyl groups of two trinuclear complexes.[12] These supramolecular assemblies can host guests, like solvent molecules or anions, in their central cavity. The ligand folding perfectly preorganizes the three metal ions in each subunit for the coordination of three facially oriented nitrogen atoms of a hexacyanometallate (Scheme 3). Indeed, the reaction of two in situ generated trinuclear complexes $[(talen^{t\text{–}Bu2})M^t_3]^{n+}$ with a hexacyanometallate $[M^c(CN)_6]^{n-6}$ results in heptanuclear complexes $\mathbf{[M^t_{6M^c}]^{n+}}$ (= $[\{(talen^{t\text{–}Bu2})M^t_3\}_2\{M^c(CN)_6\}]^{n+}$).[24] We took advantage of this molecular recognition to build an isostructural series of heptanuclear complexes by varying the central hexacyanometallate and the terminal metal ions, namely $\mathbf{[Mn^{III}_6Cr^{III}]^{3+}}$,[24,58–60] $\mathbf{[Mn^{III}_6Mn^{III}]^{3+}}$,[58,61] $\mathbf{[Mn^{III}_6Fe^{II}]^{2+}}$,[62] $\mathbf{[Mn^{III}_6Fe^{III}]^{3+}}$,[62,63] $\mathbf{[Mn^{III}_6Co^{III}]^{3+}}$,[64] $\mathbf{[Mn^{III}_6Os^{II}]^{2+}}$,[65] $\mathbf{[Mn^{III}_6Os^{III}]^{3+}}$, and $\mathbf{[Fe^{III}_6Cr^{III}]^{3+}}$.[66] Most of these complexes exhibit a slow relaxation of the magnetization. For example, $\mathbf{[Mn^{III}_6Mn^{III}]}$(lactate)$_3$ shows a hysteretic opening of ± 10 T.[61] Here we want to focus only on the $\mathbf{[Mn^{III}_6Cr^{III}]^{3+}}$ SMMs.[24,26,59]

The molecular structure of $\mathbf{[Mn^{III}_6Cr^{III}]^{3+}}$ is shown in Figure 1a. The high driving force for the supramolecular assembly allowed us to synthesize and crystallize $\mathbf{[Mn^{III}_6Cr^{III}]^{3+}}$ in form of different salts and solvates and to study the effect of molecular and crystal symmetry on the magnetic properties for the same complex in different surroundings.[58,59] As intended by the use of the triplesalen ligand, all complexes contain an approximate C_3 axis, pinching through the central phloroglucinol units and the Cr^{III} ion of the hexacyanochromate. However, most molecules do not crystallize with crystallographically imposed C_3 symmetry, which on the first hand lowers the molecular symmetry. This goes with different occupation of the sixth coordination site of the Mn^{III} ions. In analogy to mononuclear Mn^{III} salen complexes, this position can be empty or occupied by a coordinating solvent molecule. Besides this lowering of the molecular C_3 symmetry, the low crystal symmetry provides a non-symmetric environment around the molecules and a non-collinear alignment of the approximate molecular C_3 axes. This results in stray fields from neighboring SMMs with transversal field components inducing QTM. We used the frequent appearance of high symmetric space groups in compounds containing rod-shaped entities[67] to induce a high crystallographic symmetry into our system.[59] Thus, using lactate as anion $\mathbf{[Mn^{III}_6Cr^{III}]}$(lactate)$_3$ crystallized in the trigonal space group *R*. [59]

Although, the high molecular and crystal symmetry in $\mathbf{[Mn^{III}_6Cr^{III}]}$(lactate)$_3$ enforces magnetic hysteresis with almost complete suppression of QTM[26] the blocking temperatures of our SMMs do not exceed 2 K. To understand in detail the reason for these low blocking temperatures so that we were able to rationally improve our SMMs, we have analyzed the structural, spectroscopic, and magnetic properties of all our extended phloroglucinol-based complexes in detail.[68]

All trinuclear Cu^{II} complexes with our extended phloroglucinol ligands exhibit the expected ferromagnetic interactions via the spin-polarization mechanism.[7,10,12,15,16,69,70] Ferromagnetic interactions could also be established between V^{IV},[13] Ni^{II} (S = 1),[17] Co^{II} l.s.[71] and Fe^{III} l.s.[72] ions. However, the interactions between Mn^{III}[11,14,73,74] and Fe^{III}[75,76] ions through the extended phloroglucinol ligands are antiferromagnetic.

We have also analyzed the magnetic properties of all our $\mathbf{[M^t_{6M^c}]^{n+}}$ complexes, using the coupling scheme shown in Scheme 4 for $\mathbf{[Mn^{III}_6Cr^{III}]^{3+}}$. The coupling constant $J_{Mn\text{-}Mn}$ describes the exchange between Mn^{III} ions in one triplesalen subunit and $J_{Mn\text{-}Cr}$ describes the exchange between these Mn^{III} ions and the central Cr^{III} ion along the cyanide linkers. We found that the exchange between the terminal ions (either Mn^{III} or Fe^{III}) in a triplesalen subunit is always, as observed in the trinuclear Mn^{III} complexes, antiferromagnetic. In the $\mathbf{[Mn^{III}_6Cr^{III}]^{3+}}$ SMMs, the $J_{Mn\text{-}Mn}$ coupling between the Mn^{III} ions within the triplesalen-subunits is antiferromagnetic in the order of –0.7 to $^{-1}$ cm^{-1} despite our intention to enforce ferromagnetic interactions via the spin-polarization mechanism. On the other hand, the coupling via the cyanide linker is antiferromagnetic $J_{Mn\text{-}Cr}$ = –3 to –5 cm^{-1} as it is known for the Mn^{III}-C≡N-Cr^{III} coupling.[77]

Minireview
doi.org/10.1002/ejic.202000507

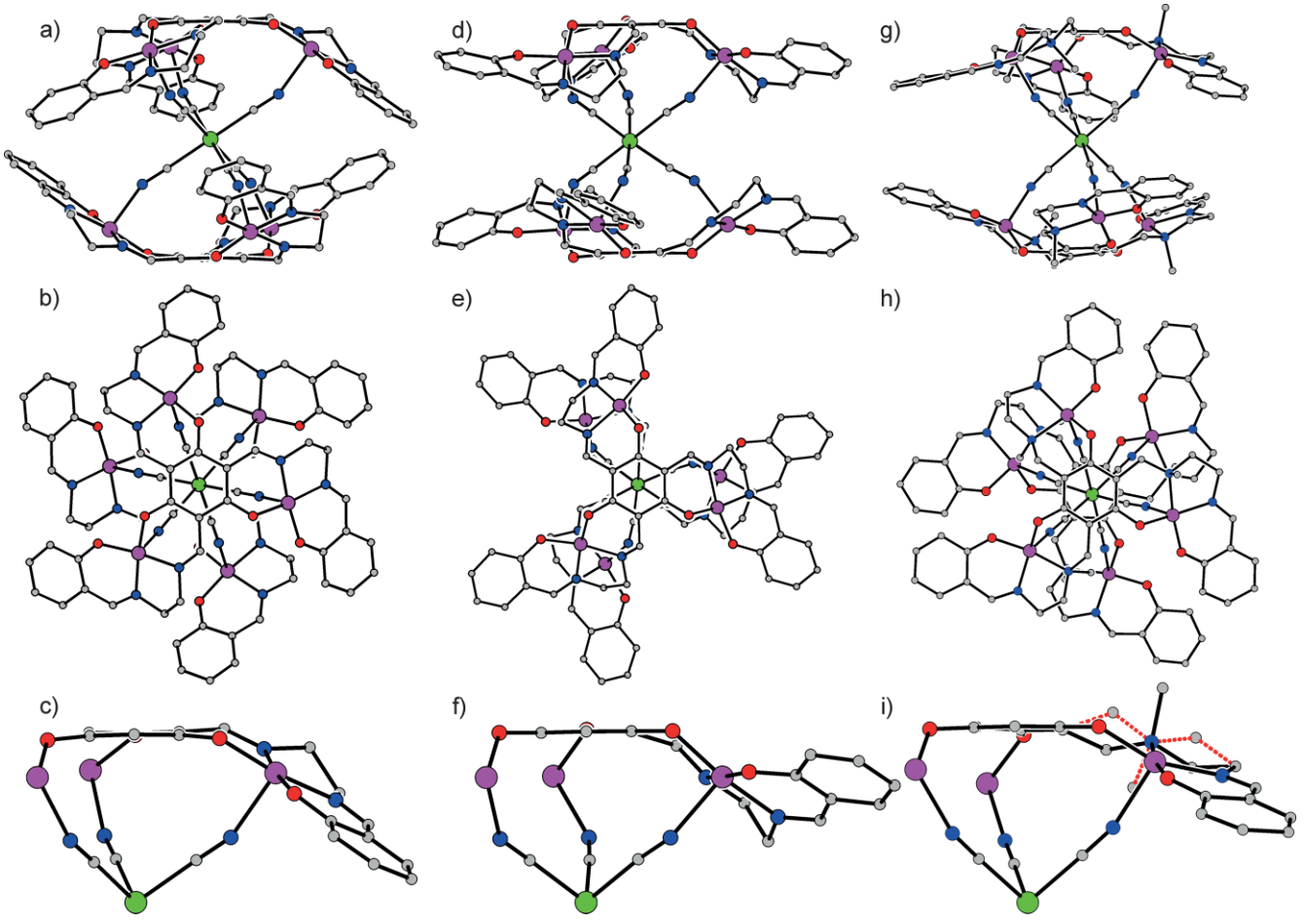

Figure 1. Comparison of the molecular structures of (a–c) **[Mn$^{III}_6$Cr^{III}]$^{3+}$** in crystals of [{(talen^{t-Bu2})Mn$^{III}_3$}$_2${Cr^{III}(CN)6}(MeOH)$_3$(CH$_3$CN)$_2$](BPh$_4$)$_3$•4CH$_3$CN•2Et$_2$O,[24] (d–f) **^{RR}[Mn$^{III}_6$Cr^{III}]$^{3+}$** in crystals of [{(chand^{RR})$_2$Mn$^{III}_6$(THF)$_{5.5}$(MeOH)$_{0.5}${Cr^{III}(CN)$_6$}](ClO$_4$)$_3$•MeOH•1.5THF•1.5Et$_2$O (reproduced with permission from ref.[83] Copyright 2017, American Chemical Society.), and (g, h) ***[Mn$^{III}_6$Cr^{III}]$^{3+}$** in crystals of [{(talalen^{t-Bu2})Mn$^{III}_3$}$_2${Cr^{III}(CN)$_6$}](BPh$_4$)$_3$•2CH$_3$CN•*t*BuOH•4Et$_2$O.[88] Some group of atoms (that is, *t*Bu, CH$_3$ (except N-CH$_3$), (CH$_2$)$_4$, and coordinated solvent molecules) and all hydrogen atoms have been omitted for the sake of clarity. (c, f, and i) show sections of the molecular structures to illustrate the variation of the local Mn^{III} coordination environments. Red dotted bonds in (i) correspond to the disordered saturated amine.

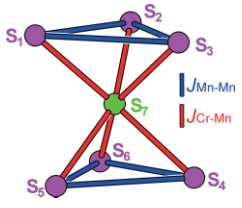

Scheme 4. Coupling scheme to analyze magnetic properties of the **[Mn$^{III}_6$Cr^{III}]$^{3+}$** SMMs.

The stronger $J_{Mn\text{-}Cr}$ enforces that all Mn^{III} spins are aligned antiparallel to the central Cr^{III} spin so that all Mn^{III} spins are oriented parallel to each other, resulting in a total spin ground state of S_t = 21/2. As will be described in more detail below, the competing antiferromagnetic $J_{Mn\text{-}Mn}$ interaction tends to align the Mn^{III} spins antiparallel, which destabilizes the spin ground state and thereby enables mixing with excited spin states. This mixing opens pathways for QTM and thus reduces the effective barrier U_{eff} for spin reversal.

This discovery triggered intensive research in our group to understand the reasons behind the failing of the spin-polarization mechanism to enforce ferromagnetic couplings. From the careful evaluation of the structural and spectroscopic properties of our extended phloroglucinol ligands and complexes we figured out that all our extended phloroglucinol ligands are actual nonaromatic heteroradialenes.

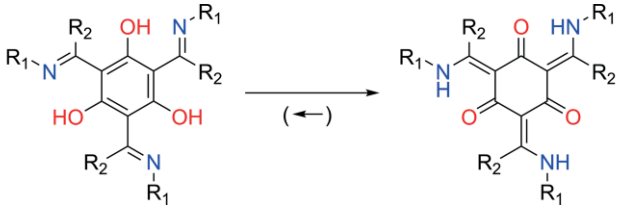

The complexes form resonance hybrids of the delocalized aromatic phloroglucinol form and the nonaromatic heteroradialene form.[16,68,69,78–80] As an efficient spin-polarization requires a delocalized aromatic bridge, the non-aromatic heteroradialene contribution suppresses spin-polarization and hence

the ferromagnetic interactions. We have identified structural as well as FTIR, NMR, and UV/Vis-NIR spectroscopic signatures that allows us to qualitatively estimate the heteroradialene contribution in the complexes.

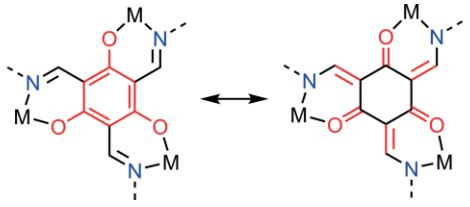

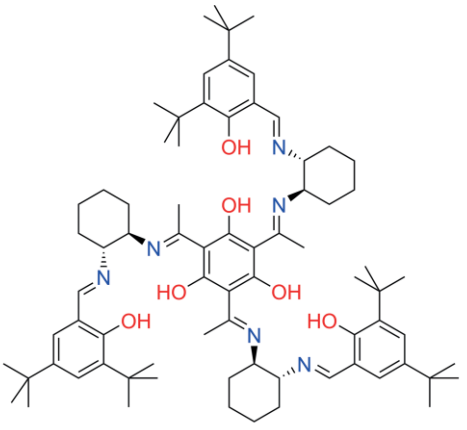

H_6chand^{RR}

5. Higher Generation Ligands to Suppress Quantum Tunneling of Magnetization

The theoretical considerations provided above for the QTM probability consider only the spin ground state of a SMM, while energetically higher spin states are neglected. This effective or giant spin approximation is only a crude description for most polynuclear SMMs with a multitude of spin states as was shown e.g. for the salicyl aldoximine SMMs **Mn_3** and **Mn_6**.[81] The mixing of higher spin states into the spin ground state (inter-state mixing) is stronger, the smaller the separations between the spin states are. The energy separation between the spin states are governed by the exchange coupling *J*, which is thereby coupled to the relaxation properties of an SMM.

Our strategy to improve our **$[Mn^{III}_6Cr^{III}]^{3+}$** SMMs was to enforce the initially intended ferromagnetic $J_{Mn\text{-}Mn}$ coupling. This should better stabilize the S_t = 21/2 groundstate and reduce inter-state mixing that opens QTM pathways. Moreover, by suppressing competing interactions, the wavefunctions are better described by a dominant M_S contribution, that reduces the tunnel splitting and lowers the QTM possibility. In order to implement this strategy to optimize our **$[Mn^{III}_6Cr^{III}]^{3+}$** SMMs, we followed three different approaches. This possibility can be regarded as a major advantage of our approach using a modular ligand system that can be rationally optimized to newly derived structure-function correlations with the versatile toolbox of organic chemistry.

However, the first approach originates from a serendipitous observation. With regards to the great success of chiral salen complexes in enantioselective catalysis for a multitude of organic reactions,[2,3] we had developed the chiral triplesalen ligand H_6chand^{RR} for applications in enantioselective catalysis:[73,75]

The trinuclear complexes $[(chand^{RR})M^{III}_3]^{3+}$ can also be used as molecular building blocks for heptanuclear complexes of the general formula $^{RR}[M^t_{6M^c}]^{n+}$ (= $[\{(chand^{RR})M^t_3\}_2\{M^c(CN)_6\}]^{n+}$, please note that the upper index ^{RR} is used to differentiate the heptanuclear complexes of the ligand $(chand^{RR})^{6-}$ from the heptanuclear complexes of the ligand $(talen^{t\text{-}Bu2})^{6-}$ that are lacking this upper index). Interestingly, the two complexes $^{RR}[Mn^{III}_6Fe^{II}]^{2+}$ and $^{RR}[Fe^{III}_6Fe^{II}]^{2+}$ with a central diamagnetic Fe^{II} l. s. exhibit ferromagnetic interactions between the Mn^{III} and Fe^{III} ions, respectively, within the trinuclear subunits through the bridging triplesalen ligand.[82] Thus, we synthesized the heptanuclear $^{RR}[Mn^{III}_6Cr^{III}]^{3+}$ with the chiral ligand $(chand^{RR})^{6-}$ as a candidate for a heptanuclear complex with a ferromagnetic $J_{Mn\text{-}Mn}$.[83]

The second approach followed the rationale that the most ferromagnetic exchange coupling observed through phloroglucinol in the Mo^V_3 complex (J = 7.2 cm^{-1})[48] is still three orders of magnitude smaller than estimated values for *meta*-phenylene bridged organic radicals and carbenes.[19,84] In these organic compounds, the spin density in the p_z orbitals is well suited for delocalization into the aromatic ring. Thus, we thought to increase the spin-delocalization from the metal ion into the aromatic ring by going from extended phloroglucinol to thiophloroglucinol ligands as the M–S bond is much more covalent than the corresponding M–O bonds. Moreover, we thought to suppress the heteroradialene formation that would require less stable C=S double bonds.

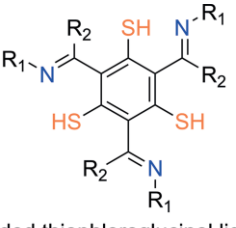

extended thiophloroglucinol ligands

A number of trinuclear Ni^{II}_3 complexes with extended thiophloroglucinol ligands allowed us to investigate their heteroradialene signatures and provided the unexpected result that the extended thiophloroglucinol derivatives possess the same amount of heteroradialene character.[80,85] Using the ligand $(habbi)^{6-}$, we could synthesize the trinuclear Cu^{II}_3 complex $[(habbi)Cu^{II}_3]$.[86]

Again, a strong heteroradialene contribution was found that suppresses an efficient spin-polarization mechanism. But importantly, the strong antiferromagnetic exchange coupling constant of J = –12 cm^{-1} compared to -1 cm^{-1} in the phloroglucinol analogues demonstrates the proof of the concept of higher spin-delocalization into the ring by the thiophloroglucinol ligand. We are working on the synthesis of **$[Mn^{III}_6Cr^{III}]^{3+}$** complexes with these extended thiophloroglucinol ligands.

Minireview
doi.org/10.1002/ejic.202000507

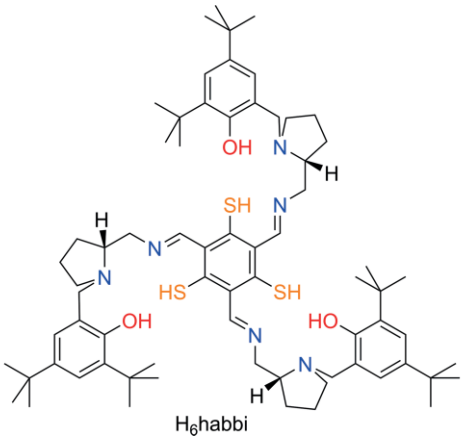

The third strategy to avoid the heteroradialene formation follows the rational that a heteroradialene requires C=N double bonds in 2,4,6-positions. Replacing the C=N double bonds by C–N single bonds should impede the heteroradialene formation.

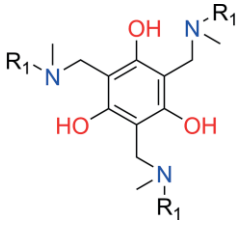

This required a completely new synthetic approach but we were successful in the synthesis of the triplesalalen ligand H_6talalen$^{t\text{–}Bu2}$ and of its heptanuclear complex [{(talalen$^{t\text{–}Bu2}$)-Mn^{III}_3}$_2${$Cr^{III}(CN)_6$}]$^{3+}$ (= ***[Mn$^{III}_6$Cr^{III}]$^{3+}$**, please note that the upper index * is used to differentiate the heptanuclear complexes of the ligand (talalen$^{t\text{–}Bu2}$)$^{6-}$ from those of the ligand (chand^{RR})$^{6-}$ that are denoted with a an upper index **RR** and those of the (talen$^{t\text{–}Bu2}$)$^{6-}$ that are lacking an upper index).[87,88]

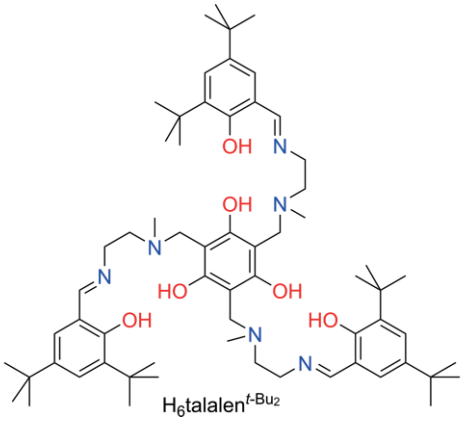

In summary, we have been able to synthesize the chiral triplesalen complex **^{RR}[Mn^{III}Cr^{III}]$^{3+}$** and the triplesalalen complex ***[Mn$^{III}_6$Cr^{III}]$^{3+}$** as candidates to improve the SMM properties of our parent **[Mn$^{III}_6$Cr^{III}]$^{3+}$** SMM. In the following the differences in their structures and magnetic properties will be analyzed and discussed with regards to suppression of QTM.

6. Structural Properties of Higher Generation [Mn$^{III}_6$Cr^{III}]$^{3+}$ Single-Molecule Magnets

The molecular structures of **[Mn$^{III}_{6Cr}$^{III}]$^{3+}$**, **^{RR}[Mn$^{III}_{6Cr}$^{III}]$^{3+}$**, and ***[Mn$^{III}_{6Cr}$^{III}]$^{3+}$** are compared in Figure 1. All three complexes are built up by the combination of two trinuclear Mn^{III}_3 complexes with a central hexacyanochromate. Substitution of the imine donors in H_6talen$^{t\text{–}Bu2}$ with *tert*-amines in H_6talalen$^{t\text{–}Bu2}$ introduced six new stereo centers at the *tert*-amines in ***[Mn$^{III}_6$Cr^{III}]$^{3+}$**. The methyl groups of the *tert*-amines can either point in the direction of the central Cr^{III} (inside) or in the opposite direction (outside) accompanied with a change of the configuration of the neighboring ethylene spacer (λ or δ). In the crystal structure, a disorder of all possible diastereomers is found but could be resolved.

In analyzing the switch from antiferromagnetic to ferromagnetic through the triplesalen ligand in the chiral **^{RR}[Mn$^{III}_{6Fe}$^{II}]$^{2+}$** and **^{RR}[Fe$^{III}_{6Fe}$^{II}]$^{2+}$** complexes, we have recognized a chirality-induced symmetry reduction.[82] The complexes **[M$^t_6$M^c]$^{n+}$** of the achiral ligand (talen$^{t\text{–}Bu2}$)$^{6-}$ contain an idealized C_3 axis and a center of inversion resulting in the point group S_6. Although the ligand is achiral, the bowl-shaped trinuclear building blocks [(talen$^{t\text{–}Bu2}$)M$^t_3$]$^{3+}$ are chiral. The inversion center requires the presence of both enantiomers in one heptanuclear complex. This is impossible by using the chiral ligand (chand^{RR})$^{6-}$ and enforces a different wrapping of the two chiral [(chand^{RR})M$^t_3$]$^{3+}$ building blocks around the central hexacyanometallate with a strong influence on the ligand folding. The chiral complexes **^{RR}[M$^t_{6M}$^{c}]$^{3+}$** possess an idealized C_3 axis but instead of a center of inversion 3 C_2 axes perpendicular to the main C_3 axis, resulting in the point group D_3. The difference is best pictured in Figure 1b and Figure 1e. The salen ligand compartments are tetradentate, coordinating in the *trans*-configuration. In this respect, they are similar to macrocyclic ligands with the difference that they are open at the phenolate O atoms ("O_2-openings"). In the parent **[Mn$^{III}_{6Cr}$^{III}]$^{3+}$** (Figure 1b), the "O_2-openings" of the salen compartments of the top and bottom [(talen$^{t\text{–}Bu2}$)Mn^{III}_3]$^{3+}$ building blocks point in one direction of rotation in accordance to a S_6 axis, while in **^{RR}[Mn$^{III}_{6Cr}$^{III}]$^{3+}$** (Figure 1e) these "O_2-openings" of the top and bottom [(chand^{RR})Mn^{III}_3]$^{3+}$ building blocks point in opposite directions of rotation in accordance to the three C_2 axes perpendicular to the C_3 main axis.

Initially we drew the hypothesis, that this symmetry reduction could be the reason for the different magnetic properties of **^{RR}[Mn$^{III}_{6Cr}$^{III}]$^{3+}$** compared to **[Mn$^{III}_{6Cr}$^{III}]$^{3+}$**.[83] Later on, we varied counterions during crystallization of **[Mn$^{III}_{6Cr}$^{III}]$^{3+}$** to obtain a compound more stable to exposure of soft X-ray radiation on gold surfaces.[89] Serendipitously, this **[Mn$^{III}_{6Cr}$^{III}]**$(ClO_4)_3$ complex crystallized with an approximate D_3 symmetry. This D_3-**[Mn$^{III}_{6Cr}$^{III}]**$(ClO_4)_3$ complex shows almost identical behavior compared to the S_6 symmetric **[Mn$^{III}_{6Cr}$^{III}]$^{3+}$** complexes.[90] Thus, the ferromagnetic coupling in the trinuclear subunits [(chand^{RR})Mn^{III}_3]$^{3+}$ cannot be ascribed to its different molecular symmetry, but has to originate from the specific properties of the chiral triplesalen ligand (chand^{RR})$^{6-}$.

Apart from the molecular symmetry, the chiral ligand (chand^{RR})$^{6-}$ induces a significantly different ligand folding of the salen subunits. Salen complexes are usually not flat molecules

but the phenolates bend from the idealized MN_2O_2 coordination plane. In trinuclear triplesalen complexes, there are six different ligand folding directions possible:[10,12] for each of the three salen-subunit one for the central phenolates (the phloroglucinol backbone) and one for the terminal phenolates. Interestingly, we always found one regular kind of ligand folding in the $[M^t_6M^c]^{n+}$ complexes of $(talen^{t\text{-}Bu2})^{6-}$. From the phloroglucinol plane, the three MN_2O_2 planes are bend in the same direction and the terminal phenolates bend also in this direction (Figure 1c), resulting in an overall "bowl-shaped" structure of the trinuclear building block (Figure 1a). In contrast, the terminal phenolates in the chiral $^{RR}[M^t_6M^c]^{n+}$ complexes of $(chand^{RR})^{6-}$ bend to the opposite direction (Figure 1f) resulting in an overall "soup-plate" structure of the trinuclear building blocks (Figure 1d). The chiral triplesalen complex $*[Mn^{III}_{6Cr}{}^{III}]^{3+}$ also shows a "bowl-shaped" structure (Figure 1g, i). For quantification we use the bend angle φ that describes the folding along the vector of two adjacent N and O donor atoms, either for the central phloroglucinol ring (φ^{ent}) or the terminal phenolates (φ^{term}) bending (Table 1). The angle θ describes the helical distortion or twisting between the best plane defined by central phloroglucinol and the vector through the central N and O donor atoms.

Table 1. Mean values of selected structural parameters for the heptanuclear complexes $[Mn^{III}_6Cr^{III}]^{3+}$, $^{RR}[Mn^{III}_6Cr^{III}]^{3+}$, and $*[Mn^{III}_6Cr^{III}]^{3+}$.

	$[Mn^{III}_6Cr^{III}]^{3+}$[e]	$^{RR}[Mn^{III}_6Cr^{III}]^{3+}$[f]	$*[Mn^{III}_6Cr^{III}]^{3+}$[g]
$\bar{d}(Mn\text{-}O)^{cent}$ / Å	1.90	1.88	1.87
$\bar{d}(Mn\text{-}O)^{term}$ / Å	1.87	1.88	1.87
$\bar{d}(Mn\text{–}N)^{cent}$ / Å	1.96	2.02	2.08
$\bar{d}(Mn\text{–}N)^{term}$ / Å	1.98	1.97	1.98
$\bar{d}(Mn\text{–}N^{C=N})$ / Å	2.18	2.23	2.17
$\bar{d}(Mn\text{–}X^{6th})$ / Å	2.49	2.43	2.50[h]
$\bar{d}(C\text{-}O)^{cent}$	1.31	1.32	1.35
$\bar{d}(C\text{-}C)^{cent}$	1.42	1.42	1.40
$HOMA^{cent}$[a]	0.68	0.77	0.94
$\bar{d}(Cr\text{–}C)$ / Å	2.07	2.07	2.07
$\bar{d}(C\equiv N)$ / Å	1.15	1.15	1.15
∠(Cr–C≡N) / °	176.1	173.3	175.8
∠(C≡N–Mn) / °	161.3	143.9	165.3
∠(C–Cr–C) / °	88.7	93.3	88.9
φ^{cent} / ° [b]	46.7	18.3	43.8
φ^{term} / ° [b]	8.5	–22.6	9.7
θ / ° [c]	1.3	25.9	11.6
ϑ / ° [d]	39.0	39.8	35.7

[a] HOMA (harmonic oscillator model of aromaticity) value that takes a value of 1 for the model aromatic system benzene and of 0 for a model non-aromatic system.[91] [b] Bent angle $\varphi = 180° - \angle(Mn\text{–}X_{NO}\text{-}X_R)$ with X_{NO}: midpoint of adjacent N and O donor atoms and X_R: midpoint of the six-membered chelate ring containing the N and O donor atoms. [c] Angle between the benzene plane of the central phloroglucinol and the vector formed by the central phenolate O atom and the central N atom. [d] Angle between the local Mn^{III} Jahn–Teller-axes and the molecular C_3 axis. [e] $[\{(talen^{t\text{-}Bu2})Mn^{III}_3\}_2\{Cr^{III}(CN)_6\}(MeOH)_3(CH_3CN)_2](BPh_4)_3\cdot 4CH_3CN\cdot 2Et_2O$.[24] [f] $[\{(chand^{RR})_2Mn^{III}_6(THF)_{5.5}(MeOH)_{0.5}\{Cr^{III}(CN)_6\}\](ClO_4)_3\cdot MeOH\cdot 1.5THF\cdot 1.5Et_2O$.[83] [g] $[\{(talalen^{t\text{-}Bu2})Mn^{III}_3\}_2\{Cr^{III}(CN)_6\}](BPh_4)_3\cdot 2CH_3CN\cdot t BuOH\cdot 4Et_2O$.[88] [h] Only one of six Mn^{III} ions has a sixth ligand.

While for $[Mn^{III}_6Cr^{III}]^{3+}$ and $*[Mn^{III}_6Cr^{III}]^{3+}$ the ligand folding along the central N–O vector (φ^{cent}) is around 45°, it is less distinct in $^{RR}[Mn^{III}_6Cr^{III}]^{3+}$ with φ^{cent} = 18.3° (Table 1). The terminal bending (φ^{term}) is around 10° in $[Mn^{III}_6Cr^{III}]^{3+}$ and $*[Mn^{III}_6Cr^{III}]^{3+}$ and thereby points in the same direction as the central bending (Figure 1f, i) forming the "bowl-shaped" structure. Contrary, the terminal bending in $^{RR}[Mn^{III}_6Cr^{III}]^{3+}$ is φ^{term} = –22.6°, where the negative sign expresses the bending in the other direction with respect to the MnN_2O_2 coordination plane (Figure 1f), forming the observed "soup plate" shaped structure. Another parameter describing the different wrapping of the chiral ligand $(chand^{RR})^{6-}$ in $^{RR}[Mn^{III}_6Cr^{III}]^{3+}$ is the helical distortion angle θ that is much larger in $^{RR}[Mn^{III}_6Cr^{III}]^{3+}$ compared to $[Mn^{III}_6Cr^{III}]^{3+}$ and intermediate in $*[Mn^{III}_6Cr^{III}]^{3+}$.

7. Determination of Heteroradialene Contributions

The amount of heteroradialene contribution for the improved complexes can be investigated especially by the central C-O bond length, correlated to the Mn-O bond length, and by the HOMA (harmonic oscillator model of aromaticity) value of the central phloroglucinol ring. The HOMA value quantifies the bond length variation in an aromatic system to distinguish a localized nonaromatic system with the value of 0 to the perfect aromatic benzene with a value of 1.[91] Compared from $[Mn^{III}_6Cr^{III}]^{3+}$ to $^{RR}[Mn^{III}_6Cr^{III}]^{3+}$ and finally $*[Mn^{III}_6Cr^{III}]^{3+}$ the central C-O bond becomes longer in line with more C-O phenolate and less C=O ketone character. The energetically higher lying $O(p_z)$ orbitals can better overlap with the Mn^{III} d orbitals, which is experimentally observed by a shortening of the Mn-O bonds. In contrast, the terminal Mn-O bonds are almost unaffected. This effect is even more pronounced for $Mn\text{-}N^{cent}$, reflecting the change from anionic amide to *tert*-amine. Additionally, the HOMA value increases in the same direction, giving a high aromatic value of 0.94 for $*[Mn^{III}_6Cr^{III}]^{3+}$. These structural parameters clearly show the increasing aromatic character of the central phloroglucinol from $[Mn^{III}_6Cr^{III}]^{3+}$ to $^{RR}[Mn^{III}_6Cr^{III}]^{3+}$ and to $*[Mn^{III}_6Cr^{III}]^{3+}$.

FT-IR spectroscopy is also well suited to identify the heteroradialene character.[76,79] $[Mn^{III}_6Cr^{III}]^{3+}$ complexes show intense features for the exocyclic ν(C=C) and ν(C=O) at around 1540 and 1490 cm^{-1}, respectively. Both features vanish completely in the spectrum of $*[Mn^{III}_6Cr^{III}]^{3+}$, further proving the absence of a heteroradialene contribution in the central phloroglucinol. $^{RR}[Mn^{III}_6Cr^{III}]^{3+}$ on the other hand still show the features of the heteroradialene, but with a shift of the ν(C=C) band to lower energies. This indicates a weakened, but still present heteroradialene contribution in $^{RR}[Mn^{III}_6Cr^{III}]^{3+}$ in accordance with the structure data.

In the UV/Vis spectra, we identified two intense features between 25000–35000 cm^{-1} as characteristic for the heteroradialene.[68,76,78,80] Figure 2 shows a decrease of intensity in this spectral region in the order $[Mn^{III}_6Cr^{III}]^{3+}$, $^{RR}[Mn^{III}_6Cr^{III}]^{3+}$, $*[Mn^{III}_6Cr^{III}]^{3+}$, which is manifested in the difference spectra. The difference of the spectra of $[Mn^{III}_6Cr^{III}]^{3+}$ and $^{RR}[Mn^{III}_6Cr^{III}]^{3+}$ is remarkable as the ligands $H_6talen^{t\text{-}Bu2}$ and H_6chand^{RR} show almost superimposable UV/Vis spectra. This clearly shows the reduction to the heteroradialene contribution also in solution.

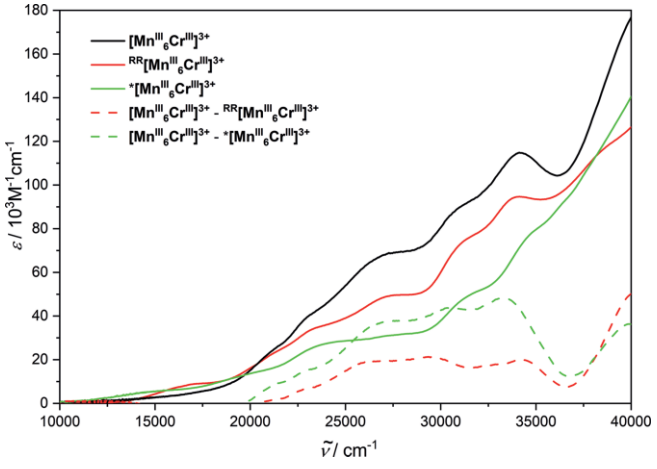

Figure 2. Electronic absorption spectra of **[Mn$^{III}_6$Cr^{III}]$^{3+}$**, **^{RR}[Mn$^{III}_6$Cr^{III}]$^{3+}$**, and ***[Mn$^{III}_6$Cr^{III}]$^{3+}$** measured in CH_3CN solutions (solid lines). For comparison, the difference spectra for the higher generation **[Mn$^{III}_6$Cr^{III}]$^{3+}$** to the parent **[Mn$^{III}_6$Cr^{III}]$^{3+}$** complex are provided (broken lines).

8. Magnetic Properties of the Higher Generations [Mn$^{III}_{6Cr}$^{III}]$^{3+}$

The magnetic properties of **[Mn$^{III}_6$Cr^{III}]$^{3+}$**, **^{RR}[Mn$^{III}_6$Cr^{III}]$^{3+}$**, and ***[Mn$^{III}_6$Cr^{III}]$^{3+}$** have been studied in detail by DC and AC magnetic measurements. Figure 3 compares representatively the temperature-dependency of μ_{eff} and variable temperature-variable field (VTVH) measurements. The decrease with decreasing temperature followed by an intense increase at about 50 K is a typical behavior for a ferrimagnetic coupling scheme The VTVH data show a strong nesting behavior, indicative for magnetically anisotropic spin ground states.

The temperature-dependence of μ_{eff} and the VTVH data were simulated simultaneously by a full-matrix diagonalization of the multi-spin Hamiltonian Equation (3) including isotropic HDvV exchange in Equation (4), zero-field splitting, and Zeeman interaction. The HDvV Hamiltonian corresponds to the coupling scheme in Scheme 4.

$$\hat{H} = \hat{H}_{HDvV} + \sum_i D_i \left(\hat{\mathbf{S}}_i \cdot \mathbf{e}_i(\vartheta_i, \varphi_i)\right)^2 + \mu_B \sum_i \mathbf{B} \cdot \underline{\underline{\mathbf{g}}}_i \cdot \hat{\mathbf{S}}_i \quad (3)$$

$$\hat{H}_{HDvV} = -2J_{Cr\text{-}Mn}\left(\mathbf{S}_1\mathbf{S}_7 + \mathbf{S}_2\mathbf{S}_7 + \mathbf{S}_3\mathbf{S}_7 + \mathbf{S}_4\mathbf{S}_7 + \mathbf{S}_5\mathbf{S}_7 + \mathbf{S}_6\mathbf{S}_7\right) - 2J_{Mn\text{-}Mn}\left(\mathbf{S}_1\mathbf{S}_2 + \mathbf{S}_2\mathbf{S}_3 + \mathbf{S}_3\mathbf{S}_1 + \mathbf{S}_4\mathbf{S}_5 + \mathbf{S}_5\mathbf{S}_6 + \mathbf{S}_6\mathbf{S}_4\right) \quad (4)$$

It was found very important to consider the relative orientations of the individual zero-field splitting tensors (unit vectors $\mathbf{e}_i$) by the angle ϑ of the Jahn–Teller axis approximated to be along the Mn^{III}–$N^{N\equiv C}$ bonds and the molecular C_3 axis (Table 1). The spin-Hamiltonian parameters are summarized in Table 2. As already described, $J_{Mn\text{-}Cr}$ is stronger than $J_{Mn\text{-}Mn}$ so that the S_{Cr} = 3/2 is oriented antiparallel to all six S_{Mn} = 2 resulting in S_t = 21/2 ground state. The antiferromagnetic $J_{Mn\text{-}Mn}$ = –0.7 cm^{-1} in the parent **[Mn$^{III}_{6Cr}$^{III}]$^{3+}$** is changed to ferromagnetic in the triplesalalen ***[Mn$^{III}_{6Cr}$^{III}]$^{3+}$** with $J_{Mn\text{-}Mn}$ = +0.4 cm^{-1}, while it is even stronger ferromagnetic with $J_{Mn\text{-}Mn}$ = +0.8 cm^{-1} in the chiral **^{RR}[Mn$^{III}_{6Cr}$^{III}]$^{3+}$**. Interestingly, the ferromagnetic coupling constant in **^{RR}[Mn$^{III}_{6Cr}$^{III}]$^{3+}$** is twice that of ***[Mn$^{III}_{6Cr}$^{III}]$^{3+}$**, even

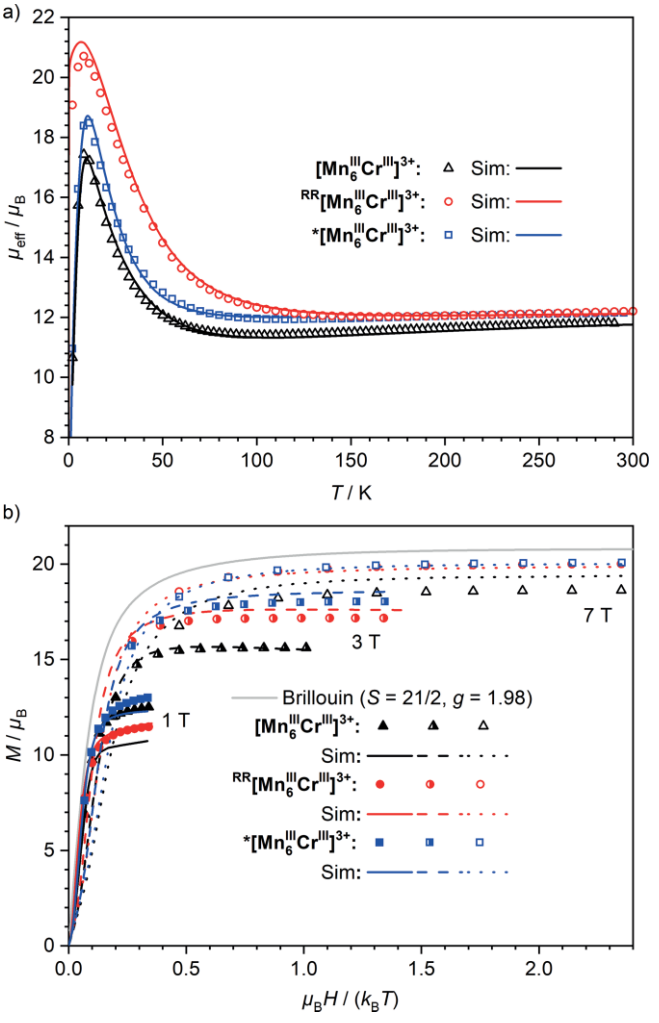

Figure 3. (a) Temperature-dependence of μeff for **[Mn$^{III}_6$Cr^{III}]$^{3+}$** (reproduced with permission from ref.[58] Copyright 2012, The Royal Society of Chemistry.) at 1 T, and **^{RR}[Mn$^{III}_6$Cr^{III}]$^{3+}$** (reproduced with permission from ref.[83] Copyright 2017, American Chemical Society.) and ***[Mn$^{III}_6$Cr^{III}]$^{3+}$** (reproduced from ref.[88]) at 0.01 T. (b) VTVH (variable temperature – variable field) magnetization measurements at 1, 3, and 7 T for **[Mn$^{III}_6$Cr^{III}]$^{3+}$** and at 1, 4, and 7 T for **^{RR}[Mn$^{III}_6$Cr^{III}]$^{3+}$** and ***[Mn$^{III}_6$Cr^{III}]$^{3+}$**. Experimental data are given as symbols. The lines correspond to simulations performed by a full-matrix diagonalization of the multi-spin Hamiltonian provided by equation (3). Parameters resulting from the simulation are provided in Table 2.

though this complex still shows a significant contribution of the heteroradialene resonance form.

The different ligand wrapping of (chand^{RR})$^{6-}$ compared to (talen$^{t\text{-}Bu2}$)$^{6-}$ and (talalen$^{t\text{-}Bu2}$)$^{6-}$ strongly change the local geometry around the Mn^{III} ions, which changes the σ- and π-contributions of the magnetic orbitals. Although we have no simple parameter to describe this complicated bonding scenario, it is very likely that these changes lead to a better overlap of the magnetic Mn^{III} d orbital with the O(p_z) orbital, resulting in a stronger spin delocalization into this orbital, which is connected with the central aromatic coupler.

The $J_{Mn\text{-}Cr}$ coupling constant of ***[Mn$^{III}_{6Cr}$^{III}]$^{3+}$** is smaller than those of **^{RR}[Mn$^{III}_{6Cr}$^{III}]$^{3+}$** and **[Mn$^{III}_{6Cr}$^{III}](BPh$_4$)$_3$** (–3.1 cm^{-1} vs. –5 cm^{-1}). This is surprising, as the ligand folding parameters for ***[Mn$^{III}_{6Cr}$^{III}]$^{3+}$** and **[Mn$^{III}_{6Cr}$^{III}]$^{3+}$** are almost identical except for

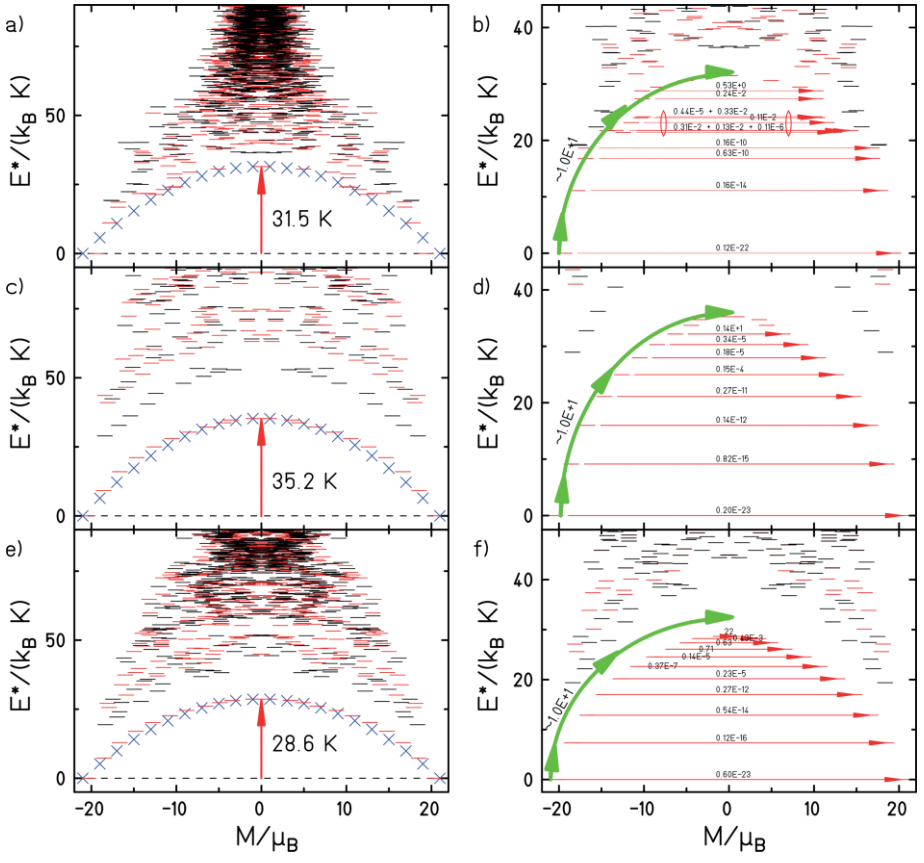

Figure 4. Magnetic energy spectrum for $[Mn^{III}_6Cr^{III}]^{3+}$ (a and b) and $^{RR}[Mn^{III}_6Cr^{III}]^{3+}$ (c and d); reproduced with permission from ref.[83] Copyright 2017, American Chemical Society; and $^{*}[Mn^{III}_6Cr^{III}]^{3+}$ (e and f; reproduced from ref.[88]) calculated by a full-matrix diagonalization of the spin Hamiltonian (Equation 3) and using the HDvV Hamiltonian (Equation 4) with the parameters provided in Table 2. Only low-lying energy levels are shown. The *x*-axis represents the magnetization of each eigenstate. *E** denotes the excitation energy (above the ground state). The blue crosses in panels a, c, and e correspond to an isolated $S = 21/2$ spin multiplet with the same barrier as of the respective complex. The eigenstates are colored by their symmetry (red, symmetric; black, antisymmetric). In panels b, d, and f, selected values of the probabilities for coherent transitions by transversal field components (QTM) are provided as thin red arrows. The bold green arrows summarize the "allowed" phonon-assisted thermal direct, Raman, and Orbach processes.

the helical distortion. This demonstrates the importance of hard-to-design specific ligand foldings for magnetic orbital overlap and hence crucial exchange interactions.

The full-matrix diagonalization approach has the important advantage to provide the energy and wavefunction of each magnetic substate. This provides important insights on the QTM pathways and relaxation properties in dependence of $J_{Mn\text{-}Mn}$. Figure 4 shows the magnetic energy spectra for the three SMMs. On the left side (Figure 4a + c + e), the energies of the lowest magnetic eigenstates are plotted as their magnetizations. For all three complexes, an anisotropy barrier is well developed. From this anisotropy barrier, the best estimation of *U* can be extracted as displayed in Figure 4 and Table 2.

The lowest substates possess magnetizations of ± 19.3 μ_B for $[Mn^{III}_6Cr^{III}]^{3+}$, ± 20.4 μ_B for $^{RR}[Mn^{III}_6Cr^{III}]^{3+}$, and ± 20.3 μ_B for $^{*}[Mn^{III}_6Cr^{III}]^{3+}$ that are close to ± 21 μ_B of the $M_S = \pm 21/2$ doublet of an isolated $S = 21/2$ spin state with $g = 2.00$. For orientation, all M_S substates of such an isolated $S = 21/2$ spin are provided as blue crosses calculated with $D_{21/2}$ to match the respective energy barriers.

For $[Mn^{III}_6Cr^{III}]^{3+}$, the ground state $S_t = 21/2$ is not separated from higher lying states. These higher lying states cannot be ascribed to $S_t = 19/2$ or 17/2 states. This is different for $^{RR}[Mn^{III}_6Cr^{III}]^{3+}$ where the $S_t = 21/2$ ground is relatively well separated from higher spin states and also the first excited $S_t = 19/2$ is relatively well behaved. $^{*}[Mn^{III}_6Cr^{III}]^{3+}$ is intermediate with a well separated $S_t = 21/2$ ground state but no separated $S_t = 19/2$ excited state.

There are several contributions leading to these energy spectra. First, the strong exchange limit ($|J| >> |D|$) is not given in

Table 2. Magnetic parameters of the heptanuclear complexes $[Mn^{III}_6Cr^{III}]^{3+}$,[59] $^{RR}[Mn^{III}_6Cr^{III}]^{3+}$,[83] $^{*}[Mn^{III}_6Cr^{III}]^{3+}$[88] obtained by full-matrix diagonalization of the multi-spin Hamiltonian provided by equations 3 and 4. Determined by simulation of the experimental μ_{eff} vs. T and VTVH data.

Compound	$[Mn^{III}_6Cr^{III}]^{3+}$[b]	$^{RR}[Mn^{III}_6Cr^{III}]^{3+}$	$^{*}[Mn^{III}_6Cr^{III}]^{3+}$
$J_{Mn\text{-}Mn}$ / cm^{-1}	−0.7±0.3	+0.8±0.1	+0.40±0.05
$J_{Mn\text{-}Cr}$ / cm^{-1}	−5.0±0.5	−5.0±0.5	−3.1±0.1
D_{MnIII} / cm^{-1}	−3.0±0.5	−3.5±0.4	−2.4±0.2
U_{eff} / K[a]	25	35	37
τ_0 / s[a]	2.6×10^{-9}	2.2×10^{-8}	6.4×10^{-9}
τ(2K) / s	7.0×10^{-4}	0.9	0.7
U / K	31.5	35.2	28.6

[a] From χ''_M vs. ω data. [b] Vacuum dried powder sample.[59]

these SMMs. Thus, excited spin states are close in energy and zero-field splitting can mix the M_S substates of different spin manifolds for all directions besides the z-direction. Another important contribution arises from the non-collinearity of local D_i tensors. In an isolated S_t = 21/2 spin, each magnetic substate can be described by a pure M_S wavefunction. This is not applicable here. The non-collinearity of the local $\boldsymbol{D}_i$ tensors in a multi-spin system results in not pure M_S wavefunctions. The basis function for this spin system can be described by $M_S|m_{S1}; m_{S2}; m_{S3}; m_{S4}; m_{S5}; m_{S6}; m_{S7}>$ with S_1–S_6 = 2 and S_7 = 3/2. A pure M_S = –21/2 substate would thus be described by –21/2|-2, –2, –2, –2, –2, –2, +3/2>. However, the contributions to the ground states contain only 42.8 % in **[Mn$^{III}_6$Cr^{III}]$^{3+}$**, 73.9 % in **^{RR}[Mn$^{III}_6$Cr^{III}]$^{3+}$**, and 71.8 % in ***[Mn$^{III}_6$Cr^{III}]$^{3+}$**. Using the same order, the second strongest contribution is 31.8 %, 13.2 %, and 15.0 % of –19/2|-1, –2, –2, –2, –2, –2, +3/2> (and all other symmetry-adapted linear combinations that will not be named here). Other basis functions that contribute in the percentage range are only summarized for further understanding: –21/2|-1, –2, –2, –2, –2, –2, +1/2>, –17/2|-1, –2, –2, –2, –2, –1, +3/2>, –21/2|-1, –2, –2, –2, –2, –2, +1/2>, and –17/2|0, –2, –2, –2, –2, –2, +3/2>. Hence, $M_S = \pm 21/2$ are not good quantum numbers for the description of the ground substates. This also explains the deviation of their magnetizations from 20.8 μ_B, the value for a pure M_S = –21/2 with g = 1.98. These mixings are even stronger for the higher magnetic substates. The higher this mixing, the lower the magnetizations, which applies specially for the substates of **[Mn$^{III}_6$Cr^{III}]$^{3+}$** above 50 K (Figure 4a).

The knowledge of the wavefunctions also allows to calculate transition probabilities for coherent transitions between the two sides of the anisotropy barrier (QTM). The spin-Hamiltonian calculations were performed in strict C_3 symmetry, hence the magnetic substates on both sides are strictly degenerated and QTM forbidden. However, there are always sources of transversal field components in a real system even if they are fluctuating. On the right side of Figure 4, tunneling probabilities induced by transversal fields are calculated for the "S_t = 21/2" ground states of the three complexes. For all three SMMs, the zero-field tunneling from "M_S = –21/2" → "M_S = +21/2" is forbidden. Significant tunneling probabilities occur between higher lying doublets (thermally assisted QTM). In **[Mn$^{III}_6$Cr^{III}]$^{3+}$**, efficient QTM pathways occur between heavily mixed states around 22–23 K, i.e. significantly below the top of the anisotropy barrier at 31.5 K. This QTM short cut coincides well with the effective barrier U_{eff} = 25 K obtained from AC measurements. For **^{RR}[Mn$^{III}_6$Cr^{III}]$^{3+}$**, the first significant short cut is closely below the top of the barrier at 32.2 K between the "$M_S = \pm 7/2$" substates. This is corroborated that U_{eff} = 35 K almost perfectly matches U = 35.2 K. ***[Mn$^{III}_6$Cr^{III}]$^{3+}$** has U = 28.6 K and the first significant QTM pathway between "$M_S = \pm 13/2$" occur around 20 K. Here, the match with U_{eff} = 37 K from AC measurements is not good. However, it must be noted, that this is a comparison between calculated values from DC magnetization simulations and experimental values obtained from an Arrhenius analysis of AC magnetization data. Thus, we would like to emphasize the perfect agreements for **[Mn$^{III}_6$Cr^{III}]$^{3+}$** and **^{RR}[Mn$^{III}_6$Cr^{III}]$^{3+}$** and not the deviations for ***[Mn$^{III}_6$Cr^{III}]$^{3+}$**.

The pair **^{RR}[Mn$^{III}_6$Cr^{III}]$^{3+}$** and ***[Mn$^{III}_6$Cr^{III}]$^{3+}$** provides an opportunity to evaluate the influence of the other spin-Hamiltonian parameters. The less strong $J_{Mn\text{-}Cr}$ (–3.1 vs. –5.0 cm^{-1}) results in smaller energetic separation of the higher spin manifolds from the "S_t = 21/2" ground state accompanied with a smaller barrier height due to the slightly reduced D_{Mn} (–2.4 vs. –3.5 cm^{-1}). These less favorable spin-Hamiltonian parameters lead to better accessible short cuts due to QTM and thus a stronger reduction from U to U_{eff}.

9. Summary and Conclusions

We have rationally designed the ligand system triplesalen to synthesize polynuclear 3d SMMs in a supramolecular approach. Although the first generation SMMs **[Mn$^{III}_6$Cr^{III}]$^{3+}$** have already a strongly reduced zero-field tunneling due to the high spin ground state S_f = 21/2 in combination with a highly symmetric molecular and crystal structure, the blocking temperatures do not exceed 2 K. For a rational improvement of our triplesalen ligand system, we needed to understand the source of this and hence analyzed the correlation between structural and spectroscopic/magnetic parameters. We have figured out that the coupling $J_{Mn\text{-}Mn}$ is antiferromagnetic and not as intended ferromagnetic via the spin-polarization mechanism through the *meta*-phenylene coupler phloroglucinol. We identified a strong contribution of a non-aromatic heteroradialene resonance structure.

Here, we have presented three different routes to overcome this problem. The first was serendipitous as the chiral triplesalen derivative H$_6$chand^{RR}, developed for enantioselective catalysis, has a lower heteroradialene contribution and a ferromagnetic $J_{Mn\text{-}Mn}$. The second route was a rational approach involving extensive organic synthesis to construct a complete new synthetic access to the thiotriplesalen ligand system starting from mesitylene. The idea was on the one hand to strengthen the electron delocalization via the more covalent M–S bond to increase the spin-polarization. On the other hand, the heteroradialene contribution was thought to be decreased due to the energetically less favorable C=S double bond contribution. However, experimentally the same heteroradialene contribution was determined for trinuclear Cu$^{II}_3$ complexes for triplesalen and thiotriplesalen complexes. But the exchange coupling in the thio derivative is an order of magnitude stronger proving the stronger spin-delocalization into the bridging ring. We are working on the synthesis of a thio derivative of **[Mn$^{III}_6$Cr^{III}]$^{3+}$**.

The last route to suppress the heteroradialene was built on the rational that a heteroradialene formation requires the presence of C=N double bonds. Thus, another new synthetic approach for the synthesis of triplesalalen ligands with C-N single bonds was established. Indeed, the triplesalalen ***[Mn$^{III}_6$Cr^{III}]$^{3+}$** has no heteroradialene character and the $J_{Mn\text{-}Mn}$ is ferromagnetic.

The knowledge of energies, wavefunctions, and QTM probabilities provides important insights into the influence of $J_{Mn\text{-}Mn}$ and of exchange couplings in general on QTM and relaxation properties of SMMs. The pair **[Mn$^{III}_6$Cr^{III}]$^{3+}$** and **^{RR}[Mn$^{III}_6$Cr^{III}]$^{3+}$** provides a good reference for the influence of $J_{Mn\text{-}Mn}$ as $J_{Mn\text{-}Cr}$

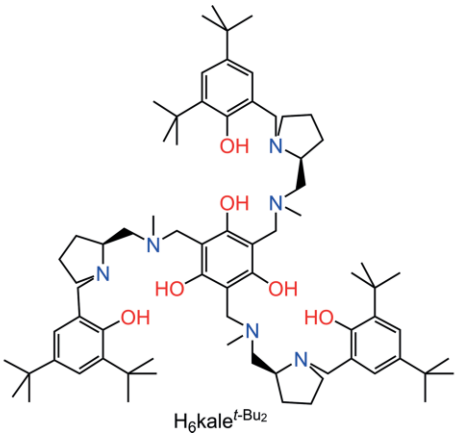

$H_6kale^{t\text{-}Bu2}$

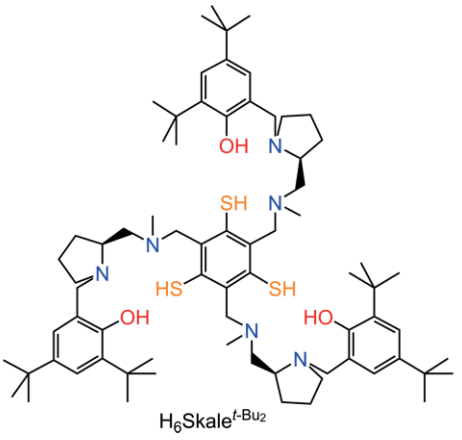

$H_6Skale^{t\text{-}Bu2}$

and D_{Mn} almost coincide. The ferromagnetic $J_{Mn\text{-}Mn}$ in $^{RR}[Mn^{III}_6Cr^{III}]^{3+}$ stabilizes the "S_t = 21/2" ground state as can be seen in Figure 4c and from the highest M_S = 21/2 contribution. In contrast, the antiferromagnetic $J_{Mn\text{-}Mn}$ not only destabilizes the "S_t = 21/2" ground but also leads to strong spin-frustration effects manifested by strong M_S = 19/2 and M_S = 17/2 contributions to the ground states wavefunctions. These effects are even stronger for the higher lying substates and open QTM pathways. Hence, U_{eff} is reduced from 35 K in $^{RR}[Mn^{III}_6Cr^{III}]^{3+}$ to 25 K in $[Mn^{III}_6Cr^{III}]^{3+}$ or from a relaxation time of 0.9 s at 2 K in $^{RR}[Mn^{III}_6Cr^{III}]^{3+}$ to 0.7 ms in $[Mn^{III}_6Cr^{III}]^{3+}$, i.e. 3 orders of magnitude decrease in relaxation times by an absolute difference in $J_{Mn\text{-}Mn}$ of only 1.5 cm^{-1}!

This shows the importance of a ferromagnetic $J_{Mn\text{-}Mn}$. For further improvements, the ligand $H_6talalen^{t\text{-}Bu2}$ without heteroradialene contribution is best suited as starting point. This ligand has two drawbacks. The terminal aldimine groups easily hydrolyze impeding the synthesis of pure samples. On the other hand, the stereo centers at the *tert*-amine ligands result in the formation of diastereomer mixtures that impedes the crystal structure analysis but more importantly reduce the C_3 symmetry. Both drawbacks are solved by the next generation ligand $H_6kale^{t\text{-}Bu2}$. The chiral terminal amine cannot hydrolyze and enforces one configuration at the central *tert*-amines. The next improvement is the thio derivative $H_6Skale^{t\text{-}Bu2}$ to provide more spin-density at the S-atom compared to the O-atoms for a stronger spin-delocalization mechanism. We are currently working on the synthesis of these next generation ligands.

In general, the optimization of SMMs should result in an increase of the blocking temperature for stabilizing a magnetization without external magnet field. This cannot be achieved by only increasing the anisotropy barrier, it also requires the suppression of QTM pathways through the anisotropy barrier. The knowledge that we have gained in our endeavors to rationally design and optimize SMMs may be summarized in a list of requirements that must be met simultaneously to rationally design and optimize SMMs:

(1) High spin ground states: A high spin ground state is not only important for increasing *U*, but also for decreasing the probability of QTM.

(2) Strong magnetic anisotropy: A strong magnetic anisotropy is mandatory for increasing *U*.

(3) Control of the molecular topology: The molecular symmetry must be at least C_3 to suppress rhombic contributions and lower than cubic. Cubic symmetry in mononuclear systems strictly generates isotropic behavior and in polynuclear systems cancels the local anisotropies by projecting onto the spin ground state. Additionally, the local anisotropy tensors should be collinear in polynuclear SMMs to maximize the anisotropy of the total spin state.

(4) Control of the crystal structure: A low symmetric crystal structure reduces the molecular symmetry. Additionally, the molecular symmetry axes must be aligned parallel to suppress transversal stray fields.

(5) Stabilization of ground state: In polynuclear complexes, the exchange coupling must be strong to isolate the ground state multiplet from excited multiplets to reduce the mixing between multiplets that reduces *U*.

Acknowledgments

We are grateful to all our co-workers mentioned in the references for their great enthusiasm and important contributions to this project. This work was supported by the DFG (FOR945 "Nanomagnets"), Fonds der Chemischen Industrie, and Bielefeld University. Open access funding enabled and organized by Projekt DEAL.

Keywords: Ligand design · Magnetic properties · Single-molecule magnets · N,O ligands · Magneto-structural correlation

[1] a) A. Werner, A. Miolati, *Z. Phys. Chem.* **1893**, *12U*, 35; b) A. Werner, A. Miolati, *Z. Phys. Chem.* **1894**, *14U*, 506; c) G. B. Kauffman, *Alfred Werner, Founder of Coordination Chemistry*, Springer Berlin Heidelberg, Berlin, Heidelberg, s.l. **1966**; d) L. H. Gade, *Chem. Unserer Zeit* **2002**, *36*, 168.
[2] T. Katsuki, *Coord. Chem. Rev.* **1995**, *140*, 189.
[3] J. F. Larrow, E. N. Jacobsen, Y. Gao, Y. Hong, X. Nie, C. M. Zepp, *J. Org. Chem.* **1994**, *59*, 1939.
[4] H. van Crawford, H. W. Richardson, J. R. Wasson, D. J. Hodgson, W. E. Hatfield, *Inorg. Chem.* **1976**, *15*, 2107.

[5] a) K. Srinivasan, P. Michaud, J. K. Kochi, *J. Am. Chem. Soc.* **1986**, *108*, 2309; b) W. Zhang, J. L. Loebach, S. R. Wilson, E. N. Jacobsen, *J. Am. Chem. Soc.* **1990**, *112*, 2801; c) E. G. Samsel, K. Srinivasan, J. K. Kochi, *J. Am. Chem. Soc.* **1985**, *107*, 7606.
[6] O. Kahn, *Acc. Chem. Res.* **2000**, *33*, 647.
[7] T. Glaser, M. Gerenkamp, R. Fröhlich, *Angew. Chem. Int. Ed.* **2002**, *41*, 3823; *Angew. Chem.* **2002**, *114*, 3984.
[8] T. Glaser, M. Heidemeier, T. Lugger, *Dalton Trans.* **2003**, 2381.
[9] a) T. Glaser, I. Liratzis, T. Lügger, R. Fröhlich, *Eur. J. Inorg. Chem.* **2004**, *2004*, 2683; b) T. Glaser, H. Theil, I. Liratzis, T. Weyhermüller, E. Bill, *Inorg. Chem.* **2006**, *45*, 4889; c) T. Glaser, H. Theil, M. Heidemeier, *C. R. Chim.* **2008**, *11*, 1121; d) B. Sonnenburg, I. Liratzis, A. Stammler, H. Bögge, T. Glaser, *Eur. J. Inorg. Chem.* **2015**, *2015*, 912.
[10] T. Glaser, M. Heidemeier, S. Grimme, E. Bill, *Inorg. Chem.* **2004**, *43*, 5192.
[11] T. Glaser, M. Heidemeier, R. Fröhlich, *C. R. Chim.* **2007**, *10*, 71.
[12] T. Glaser, M. Heidemeier, J. B. H. Strautmann, H. Bögge, A. Stammler, E. Krickemeyer, R. Huenerbein, S. Grimme, E. Bothe, E. Bill, *Chem. Eur. J.* **2007**, *13*, 9191.
[13] H. Theil, C.-G. Freiherr v. Richthofen, A. Stammler, H. Bögge, T. Glaser, *Inorg. Chim. Acta* **2008**, *361*, 916.
[14] T. Glaser, M. Heidemeier, H. Theil, A. Stammler, H. Bögge, J. Schnack, *Dalton Trans.* **2010**, *39-39*, 192.
[15] S. Walleck, H. Theil, M. Heidemeier, G. Heinze-Brückner, A. Stammler, H. Bögge, T. Glaser, *Inorg. Chim. Acta* **2010**, *363*, 4287.
[16] B. Feldscher, A. Stammler, H. Bögge, T. Glaser, *Dalton Trans.* **2010**, *39*, 11675.
[17] C.-G. Freiherr von Richthofen, A. Stammler, H. Bögge, T. Glaser, *Eur. J. Inorg. Chem.* **2011**, *2011*, 49.
[18] a) H. C. Longuet-Higgins, *J. Chem. Phys.* **1950**, *18*, 265; b) H. Iwamura, *Adv. Phys. Org. Chem.* **1990**, *26*, 179; c) D. A. Dougherty, *Acc. Chem. Res.* **1991**, *24*, 88; d) J. A. McCleverty, M. D. Ward, *Acc. Chem. Res.* **1998**, *31*, 842; e) Å. van Ung, S. M. Couchman, J. C. Jeffery, J. A. McCleverty, M. D. Ward, F. Totti, D. Gatteschi, *Inorg. Chem.* **1999**, *38*, 365; f) J. Cano, E. Ruiz, S. Alvarez, M. Verdaguer, *Comments Inorg. Chem.* **1998**, *20*, 27; g) I. Fernández, R. Ruiz, J. Faus, M. Julve, F. Lloret, J. Cano, X. Ottenwaelder, Y. Journaux, M. C. Muñoz, *Angew. Chem. Int. Ed.* **2001**, *40*, 3039; *Angew. Chem.* **2001**, *113*, 3129; h) E. Ruiz, J. Cirera, S. Alvarez, *Coord. Chem. Rev.* **2005**, *249*, 2649.
[19] A. Rajca, *Chem. Rev.* **1994**, *94*, 871.
[20] O. Kahn, *Inorg. Chim. Acta* **1982**, *62*, 3.
[21] a) C. Zener, *Phys. Rev.* **1951**, *82*, 403; b) G. Blondin, J. J. Girerd, *Chem. Rev.* **1990**, *90*, 1359; c) T. Glaser, K. Rose, S. E. Shadle, B. Hedman, K. O. Hodgson, E. I. Solomon, *J. Am. Chem. Soc.* **2001**, *123*, 442; d) T. Beissel, F. Birkelbach, E. Bill, T. Glaser, F. Kesting, C. Krebs, T. Weyhermüller, K. Wieghardt, C. Butzlaff, A. X. Trautwein, *J. Am. Chem. Soc.* **1996**, *118*, 12376; e) T. Glaser, F. Kesting, T. Beissel, E. Bill, T. Weyhermüller, W. Meyer-Klaucke, K. Wieghardt, *Inorg. Chem.* **1999**, *38*, 722; f) T. Glaser, T. Beissel, E. Bill, T. Weyhermüller, V. Schünemann, W. Meyer-Klaucke, A. X. Trautwein, K. Wieghardt, *J. Am. Chem. Soc.* **1999**, *121*, 2193.
[22] a) T. Jany, A. Moreth, C. Gruschka, A. Sischka, A. Spiering, M. Dieding, Y. Wang, S. H. Samo, A. Stammler, H. Bögge et al., *Inorg. Chem.* **2015**, *54*, 2679; b) T. Glaser, G. Fischer von Mollard, D. Anselmetti, *Inorg. Chim. Acta* **2016**, *452*, 62.
[23] a) J. B. H. Strautmann, S. D. George, E. Bothe, E. Bill, T. Weyhermuller, A. Stammler, H. Bogge, T. Glaser, *Inorg. Chem.* **2008**, *47*, 6804; b) J. B. H. Strautmann, C.-G. Freiherr von Richthofen, S. DeBeer George, E. Bothe, E. Bill, T. Glaser, *Chem. Commun.* **2009**, 2637; c) J. B. H. Strautmann, C.-G. Freiherr von Richthofen, G. Heinze-Brückner, S. DeBeer, E. Bothe, E. Bill, T. Weyhermüller, A. Stammler, H. Bögge, T. Glaser, *Inorg. Chem.* **2011**, *50*, 155; d) J. B. H. Strautmann, S. Walleck, H. Bögge, A. Stammler, T. Glaser, *Chem. Commun.* **2011**, *47*, 695; e) J. B. H. Strautmann, S. Dammers, T. Limpke, J. Parthier, T. P. Zimmermann, S. Walleck, G. Heinze-Brückner, A. Stammler, H. Bögge, T. Glaser, *Dalton Trans.* **2016**, *45*, 3340; f) T. Limpke, C. Butenuth, A. Stammler, H. Bögge, T. Glaser, *Eur. J. Inorg. Chem.* **2017**, *2017*, 3570; g) T. P. Zimmermann, T. Limpke, A. Stammler, H. Bögge, S. Walleck, T. Glaser, *Inorg. Chem.* **2018**, *57*, 5400; h) T. P. Zimmermann, T. Limpke, N. Orth, A. Franke, A. Stammler, H. Bögge, S. Walleck, I. Ivanovic-Burmazovic, T. Glaser, *Inorg. Chem.* **2018**, *57*, 10457; i) T. P. Zimmermann, S. Dammers, A. Stammler, H. Bögge, T. Glaser, *Eur. J. Inorg. Chem.* **2018**, *2018*, 5229; j) T. Glaser, *Coord. Chem. Rev.* **2019**, *380*, 353.
[24] T. Glaser, M. Heidemeier, T. Weyhermüller, R.-D. Hoffmann, H. Rupp, P. Müller, *Angew. Chem. Int. Ed.* **2006**, *45*, 6033; *Angew. Chem.* **2006**, *118*, 6179.
[25] T. Glaser, *Chem. Commun.* **2011**, *47*, 116.
[26] T. Glaser, V. Hoeke, K. Gieb, J. Schnack, C. Schröder, P. Müller, *Coord. Chem. Rev.* **2015**, *289–290*, 261.
[27] R. Sessoli, D. Gatteschi, A. Caneschi, M. A. Novak, *Nature* **1993**, *365*, 141.
[28] a) G. Christou, D. Gatteschi, D. N. Hendrickson, R. Sessoli, *MRS Bull.* **2000**, *25*, 66; b) M. Murrie, *Chem. Soc. Rev.* **2010**, *39*, 1986.
[29] D. Gatteschi, R. Sessoli, *Angew. Chem. Int. Ed.* **2003**, *42*, 268; *Angew. Chem.* **2003**, *115*, 278.
[30] a) T. Lis, *Acta Crystallogr., Sect. B* **1980**, *36*, 2042; b) R. Sessoli, H. L. Tsai, A. R. Schake, S. Wang, J. B. Vincent, K. Folting, D. Gatteschi, G. Christou, D. N. Hendrickson, *J. Am. Chem. Soc.* **1993**, *115*, 1804.
[31] C. Paulsen, J.-G. Park, B. Barbara, R. Sessoli, A. Caneschi, *J. Magn. Magn. Mater.* **1995**, *140–144*, 1891.
[32] a) C. J. Milios, C. P. Raptopoulou, A. Terzis, F. Lloret, R. Vicente, S. P. Perlepes, A. Escuer, *Angew. Chem. Int. Ed.* **2004**, *43*, 210; *Angew. Chem.* **2004**, *116*, 212; b) C. J. Milios, A. Vinslava, A. G. Whittaker, S. Parsons, W. Wernsdorfer, G. Christou, S. P. Perlepes, E. K. Brechin, *Inorg. Chem.* **2006**, *45*, 5272; c) C. J. Milios, A. Vinslava, W. Wernsdorfer, S. Moggach, S. Parsons, S. P. Perlepes, G. Christou, E. K. Brechin, *J. Am. Chem. Soc.* **2007**, *129*, 2754.
[33] C. J. Milios, R. Inglis, R. Bagai, W. Wernsdorfer, A. Collins, S. Moggach, S. Parsons, S. P. Perlepes, G. Christou, E. K. Brechin, *Chem. Commun.* **2007**, 3476.
[34] N. Ishikawa, M. Sugita, T. Ishikawa, S.-Y. Koshihara, Y. Kaizu, *J. Am. Chem. Soc.* **2003**, *125*, 8694.
[35] a) N. Ishikawa, M. Sugita, W. Wernsdorfer, *J. Am. Chem. Soc.* **2005**, *127*, 3650; b) K. Katoh, Y. Yoshida, M. Yamashita, H. Miyasaka, B. K. Breedlove, T. Kajiwara, S. Takaishi, N. Ishikawa, H. Isshiki, Y. F. Zhang et al., *J. Am. Chem. Soc.* **2009**, *131*, 9967; c) J. D. Rinehart, J. R. Long, *Chem. Sci.* **2011**, *2*, 2078; d) D. N. Woodruff, R. E. P. Winpenny, R. A. Layfield, *Chem. Rev.* **2013**, *113*, 5110; e) Y.-S. Meng, L. Xu, J. Xiong, Q. Yuan, T. Liu, B.-W. Wang, S. Gao, *Angew. Chem. Int. Ed.* **2018**, *57*, 4673; *Angew. Chem.* **2018**, *130*, 4763; f) K. Randall McClain, C. A. Gould, K. Chakarawet, S. J. Teat, T. J. Groshens, J. R. Long, B. G. Harvey, *Chem. Sci.* **2018**, *9*, 8492; g) Y.-C. Chen, J.-L. Liu, L. Ungur, J. Liu, Q.-W. Li, L.-F. Wang, Z.-P. Ni, L. F. Chibotaru, X.-M. Chen, M.-L. Tong, *J. Am. Chem. Soc.* **2016**, *138*, 2829; h) A. B. Canaj, S. Dey, E. R. Martí, C. Wilson, G. Rajaraman, M. Murrie, *Angew. Chem. Int. Ed.* **2019**, *58*, 14146–000; *Angew. Chem.* **2019**, *131*, 000; i) J. M. Frost, K. L. M. Harriman, M. Murugesu, *Chem. Sci.* **2016**, *7*, 2470; j) M. Gregson, N. F. Chilton, A.-M. Ariciu, F. Tuna, I. F. Crowe, W. Lewis, A. J. Blake, D. Collison, E. J. L. McInnes, R. E. P. Winpenny et al., *Chem. Sci.* **2016**, *7*, 155; k) F.-S. Guo, A. K. Bar, R. A. Layfield, *Chem. Rev.* **2019**, *119*, 8479; l) F. Pointillart, O. Cador, B. Le Guennic, L. Ouahab, *Coord. Chem. Rev.* **2017**, *346*, 150; m) B. M. Day, F.-S. Guo, R. A. Layfield, *Acc. Chem. Res.* **2018**, *51*, 1880; n) H. L. C. Feltham, S. Brooker, *Coord. Chem. Rev.* **2014**, *276*, 1.
[36] Y.-S. Ding, N. F. Chilton, R. E. P. Winpenny, Y.-Z. Zheng, *Angew. Chem. Int. Ed.* **2016**, *55*, 16071; *Angew. Chem.* **2016**, *128*, 16305.
[37] a) J. D. Rinehart, J. R. Long, *J. Am. Chem. Soc.* **2009**, *131*, 12558; b) N. Magnani, C. Apostolidis, A. Morgenstern, E. Colineau, J.-C. Griveau, H. Bolvin, O. Walter, R. Caciuffo, *Angew. Chem. Int. Ed.* **2011**, *50*, 1696; *Angew. Chem.* **2011**, *123*, 1734.
[38] a) J. M. Zadrozny, D. J. Xiao, M. Atanasov, G. J. Long, F. Grandjean, F. Neese, J. R. Long, *Nat. Chem.* **2013**, *5*, 577; b) H.-J. Lin, D. Siretanu, D. A. Dickie, D. Subedi, J. J. Scepaniak, D. Mitcov, R. Clerac, J. M. Smith, *J. Am. Chem. Soc.* **2014**, *136*, 13326; c) S. Gomez-Coca, E. Cremades, N. Aliaga-Alcalde, E. Ruiz, *J. Am. Chem. Soc.* **2013**, *135*, 7010; d) Y. Rechkemmer, F. D. Breitgoff, M. van der Meer, M. Atanasov, M. Hakl, M. Orlita, P. Neugebauer, F. Neese, B. Sarkar, J. van Slageren, *Nat. Commun.* **2016**, *7*, 10467.
[39] K. S. Pedersen, J. Dreiser, H. Weihe, R. Sibille, H. V. Johannesen, M. A. Sørensen, B. E. Nielsen, M. Sigrist, H. Mutka, S. Rols et al., *Inorg. Chem.* **2015**, *54*, 7600.
[40] a) S. Demir, M. I. Gonzalez, L. E. Darago, W. J. Evans, J. R. Long, *Nat. Commun.* **2017**, *8*, 2144; b) F.-S. Guo, B. M. Day, Y.-C. Chen, M.-L. Tong, A. Mansikkamäki, R. A. Layfield, *Angew. Chem. Int. Ed.* **2017**, *56*, 11445; *Angew. Chem.* **2017**, *129*, 11603; c) C. A. P. Goodwin, F. Ortu, D. Reta, N. F. Chilton, D. P. Mills, *Nature* **2017**, *548*, 439.

[41] F.-S. Guo, B. M. Day, Y.-C. Chen, M.-L. Tong, A. Mansikkamäki, R. A. Layfield, *Science* **2018**, *362*, 1400.
[42] A. Chiesa, F. Cugini, R. Hussain, E. Macaluso, G. Allodi, E. Garlatti, M. Giansiracusa, C. A. P. Goodwin, F. Ortu, D. Reta et al., *Phys. Rev. B* **2020**, 101, 174402.
[43] L. Thomas, F. Lionti, R. Ballou, D. Gatteschi, R. Sessoli, B. Barbara, *Nature* **1996**, *383*, 145.
[44] Friedman, Sarachik, Tejada, Ziolo, *Phys. Rev. Lett.* **1996**, *76*, 3830.
[45] R. E. P. Winpenny, *J. Chem. Soc., Dalton Trans.* **2002**, 1.
[46] R. Bagai, G. Christou, *Chem. Soc. Rev.* **2009**, *38*, 1011.
[47] K. S. Pedersen, J. Bendix, R. Clérac, *Chem. Commun.* **2014**, *50*, 4396.
[48] V. A. Ung, A. Thompson, D. Bardwell, D. Gatteschi, J. Jeffery, J. McCleverty, F. Totti, M. D. Ward, *Inorg. Chem.* **1997**, *36*, 3447.
[49] R. Boča, *Coord. Chem. Rev.* **2004**, *248*, 757.
[50] A. Bencini, D. Gatteschi, *Electron Paramagnetic Resonance of Exchange Coupled Systems*, Springer Berlin Heidelberg, Berlin, Heidelberg, **1990**.
[51] L. B. Dugad, D. V. Behere, V. R. Marathe, S. Mitra, *Chem. Phys. Lett.* **1984**, *104*, 353.
[52] K. A. Campbell, M. R. Lashley, J. K. Wyatt, M. H. Nantz, R. D. Britt, *J. Am. Chem. Soc.* **2001**, *123*, 5710.
[53] W. Wernsdorfer in *Advances in Chemical Physics*, *Vol. 118* (Eds.: I. Prigogine, S. A. Rice), J. Wiley, New York, **2001**, pp. 99–190.
[54] a) L. Landau, *Phys. Z. Sowjetunion* **1932**, *2*, 46; b) C. Zener, *Proc. R. Soc. London Ser. A* **1932**, *137*, 696; c) E. C. G. Stückelberg, *Helv. Phys. Acta* **1932**, *5*, 369.
[55] S. Miyashita, *J. Phys. Soc. Jpn.* **1995**, *64*, 3207.
[56] F. E. Mabbs, *Chem. Soc. Rev.* **1993**, *22*, 313.
[57] T. Glaser, M. Heidemeier, R. Fröhlich, P. Hildebrandt, E. Bothe, E. Bill, *Inorg. Chem.* **2005**, *44*, 5467.
[58] V. Hoeke, M. Heidemeier, E. Krickemeyer, A. Stammler, H. Bögge, J. Schnack, T. Glaser, *Dalton Trans.* **2012**, *41*, 12942.
[59] V. Hoeke, M. Heidemeier, E. Krickemeyer, A. Stammler, H. Bögge, J. Schnack, A. Postnikov, T. Glaser, *Inorg. Chem.* **2012**, *51*, 10929.
[60] A. Helmstedt, N. Dohmeier, N. Müller, A. Gryzia, A. Brechling, U. Heinzmann, V. Hoeke, E. Krickemeyer, T. Glaser, P. Leicht et al., *J. Electron Spec. Relat. Phenom.* **2015**, *198*, 12.
[61] V. Hoeke, K. Gieb, P. Müller, L. Ungur, L. F. Chibotaru, M. Heidemeier, E. Krickemeyer, A. Stammler, H. Bögge, C. Schröder et al., *Chem. Sci.* **2012**, *3*, 2868.
[62] V. Hoeke, E. Krickemeyer, M. Heidemeier, H. Theil, A. Stammler, H. Bögge, T. Weyhermüller, J. Schnack, T. Glaser, *Eur. J. Inorg. Chem.* **2013**, *2013*, 4398.
[63] T. Glaser, M. Heidemeier, E. Krickemeyer, H. Bogge, A. Stammler, R. Frohlich, E. Bill, J. Schnack, *Inorg. Chem.* **2009**, *48*, 607.
[64] E. Krickemeyer, V. Hoeke, A. Stammler, H. Bögge, J. Schnack, T. Glaser, *Z. Naturforsch. B* **2010**, *65*, 295.
[65] V. Hoeke, A. Stammler, H. Bogge, J. Schnack, T. Glaser, *Inorg. Chem.* **2014**, *53*, 257.
[66] N. Dohmeier, A. Helmstedt, N. Müller, A. Gryzia, A. Brechling, U. Heinzmann, M. Heidemeier, E. Krickemeier, A. Stammler, H. Bögge et al., *Magnetochemistry* **2016**, *2*, 5.
[67] a) M. O'Keeffe, S. Andersson, *Acta Crystallogr., Sect. A* **1977**, *33*, 914; b) E. L. Starostin, *J. Phys. Condens. Matter* **2006**, *18*, S187–S204; c) U. Steinbrenner, A. Simon, *Z. Kristallogr.* **1997**, 212; d) U. Steinbrenner, A. Simon, *Z. Anorg. Chem.* **1998**, *624*, 228; e) M. C. Schaloske, L. Kienle, H. Mattausch, V. Duppel, A. Simon, *Eur. J. Inorg. Chem.* **2011**, *2011*, 4049.
[68] T. Glaser, *Coord. Chem. Rev.* **2013**, *257*, 140.
[69] B. Feldscher, A. Stammler, H. Bögge, T. Glaser, *Polyhedron* **2011**, *30*, 3038.
[70] C.-G. Freiherr v. Richthofen, A. Stammler, H. Bögge, T. Glaser, *Eur. J. Inorg. Chem.* **2012**, *2012*, 5934.
[71] J. Oldengott, A. Stammler, H. Bogge, T. Glaser, *Dalton Trans.* **2015**, *44*, 9732.
[72] J. Oldengott, C.-G. Freiherr v. Richthofen, S. Walleck, A. Stammler, H. Bögge, T. Glaser, *Eur. J. Inorg. Chem.* **2018**, *2018*, 4987.
[73] C. Mukherjee, A. Stammler, H. Bögge, T. Glaser, *Inorg. Chem.* **2009**, *48*, 9476.
[74] E. Krickemeyer, Y. Kaiser, A. Stammler, H. Bögge, T. Glaser, *Z. Anorg. Allg. Chem.* **2013**, *639*, 1527.
[75] C. Mukherjee, A. Stammler, H. Bögge, T. Glaser, *Chem. Eur. J.* **2010**, *16*, 10137.
[76] B. Feldscher, E. Krickemeyer, M. Moselage, H. Theil, V. Hoeke, Y. Kaiser, A. Stammler, H. Bögge, T. Glaser, *Sci. China Chem.* **2012**, *55*, 951.
[77] a) H. Miyasaka, T. Madanbashi, A. Saitoh, N. Motokawa, R. Ishikawa, M. Yamashita, S. Bahr, W. Wernsdorfer, R. Clérac, *Chem. Eur. J.* **2012**, *18*, 3942; b) F. Pan, Z.-M. Wang, S. Gao, *Inorg. Chem.* **2007**, *46*, 10221.
[78] C.-G. Freiherr v. Richthofen, A. Stammler, H. Bögge, T. Glaser, *J. Org. Chem.* **2012**, *77*, 1435.
[79] C.-G. Freiherr v. Richthofen, B. Feldscher, K.-A. Lippert, A. Stammler, H. Bögge, T. Glaser, *Z. Naturforschung Sect: B* **2013**, *68*, 64.
[80] B. Feldscher, A. Stammler, H. Bögge, T. Glaser, *Chem. Asian J.* **2014**, *9*, 2205.
[81] S. Hill, S. Datta, J. Liu, R. Inglis, C. J. Milios, P. L. Feng, J. J. Henderson, E. del Barco, E. K. Brechin, D. N. Hendrickson, *Dalton Trans.* **2010**, *39*, 4693.
[82] C. Mukherjee, V. Hoeke, A. Stammler, H. Bögge, J. Schnack, T. Glaser, *Dalton Trans.* **2014**, *43*, 9690.
[83] K.-A. Lippert, C. Mukherjee, J.-P. Broschinski, Y. Lippert, S. Walleck, A. Stammler, H. Bögge, J. Schnack, T. Glaser, *Inorg. Chem.* **2017**, *56*, 15119.
[84] a) S. Kato, K. Morokuma, D. Feller, E. R. Davidson, W. T. Borden, *J. Am. Chem. Soc.* **1983**, *105*, 1791; b) P. G. Wenthold, J. B. Kim, W. C. Lineberger, *J. Am. Chem. Soc.* **1997**, *119*, 1354.
[85] B. Feldscher, H. Theil, A. Stammler, H. Bogge, T. Glaser, *Dalton Trans.* **2014**, *43*, 4102.
[86] B. Feldscher, H. Theil, A. Stammler, H. Bogge, T. Glaser, *Inorg. Chem.* **2012**, *51*, 8652.
[87] J. Donner, J.-P. Broschinski, B. Feldscher, A. Stammler, H. Bögge, T. Glaser, D. Wegner, *Phys. Rev. B* **2017**, *95*, 165441.
[88] J.-P. Venne, B. Feldscher, S. Walleck, A. Stammler, H. Bögge, J. Schnack, T. Glaser, *Chem. Eur. J.* **2019**, *25*, 4992.
[89] A. Helmstedt, M. D. Sacher, A. Gryzia, A. Harder, A. Brechling, N. Müller, U. Heinzmann, V. Hoeke, E. Krickemeyer, T. Glaser, S. Bouvron, M. Fonin, *J. Electron Spectrosc. Relat. Phenom.* **2012**, *184*, 583.
[90] V. Hoeke, A. Stammler, H. Bögge, T. Glaser, *Z. Anorg. Allg. Chem.* **2018**, *644*, 1354.
[91] J. Kruszewski, T. M. Krygowski, *Tetrahedron Lett.* **1972**, *13*, 3839.

Received: May 26, 2020